Cold Regions Science and Technology 154 (2018) 9–22

Contents lists available at ScienceDirect

Cold Regions Science and Technology

journal homepage: www.elsevier.com/locate/coldregions

Spatio-temporal maps of past avalanche events derived from tree-ring analysis: A case study in the Zermatt valley (Valais, Switzerland)

Adrien Favillier[a,*], Sébastien Guillet[b,c], Daniel Trappmann[b,c], Pauline Morel[b,c,d], Jérôme Lopez-Saez[b], Nicolas Eckert[e], Gregor Zenhäusern[f], Jean-Luc Peiry[g], Markus Stoffel[b,c,h], Christophe Corona[a]

[a] Université Clermont Auvergne, CNRS, GEOLAB, F-63000 Clermont-Ferrand, France
[b] University of Geneva, Institute for Environmental Sciences, Climate Change Impacts and Risks in the Anthropocene (C-CIA), 66 Boulevard Carl-Vogt, CH-1205 Geneva, Switzerland
[c] Dendrolab.ch, Department of Earth Sciences, University of Geneva, rue des Maraîchers 13, CH-1205 Geneva, Switzerland
[d] Univ. Grenoble Alpes, IRSTEA, UR EMGR, 38402 St-Martin-d'Hères Cedex, France
[e] Univ. Grenoble Alpes, IRSTEA, UR ETNA, 38402 St-Martin-d'Hères Cedex, France
[f] Internationales Institut zur Erforschung der Geschichte des Alpenraums, CH-3900 Brig, Switzerland
[g] CNRS, UMI3189, « Environnement, Santé, Sociétés », Faculté de Médecine, UCAD, BP 5005 Dakar-Fann, Senegal
[h] Department F.-A. Forel for Aquatic and Environmental Sciences, University of Geneva, 66 Boulevard Carl-Vogt, CH-1205 Geneva, Switzerland

A B S T R A C T

Expected runout distances and related return periods are the most important parameters needed for zoning in terrain prone to snow avalanching. Hazard mapping procedures usually allocate areas of land to zones with a different degree of danger based on return periods estimated for given snow volumes in the starting zone or with statistical/dynamical models. On forested avalanche paths, dendrogeomorphology has a great potential to add critical input data to these calculations in terms of recurrence intervals or return periods. However, quite paradoxically, recurrence interval maps of snow avalanches have only rarely been retrieved from tree-ring analysis and mostly represent the inverse of the mean frequency of avalanches that could be retrieved locally rather than the return period. The purpose of this study therefore was to propose a consistent approach for tree-ring based recurrence interval mapping of snow avalanche events. On the basis of 71 snow avalanches retrieved from 2570 GD growth disturbances identified in 307 larch trees from three avalanche paths located in the vicinity of Täsch (Canton of Valais, Swiss Alps), we first followed the classical approach used in dendrogeomorphology and derived recurrence interval maps through interpolation from recurrence intervals observed at the level of individual trees. We then applied an expert delineation of the spatial extent of past events based on the location of disturbed trees. Our results show that the second step improved representation of expected patterns of recurrence intervals that typically increase as one moves down the centerline of the avalanche path. Despite remaining limitations and uncertainties precluding from direct use of our maps for hazard mapping purpose, these results suggest that dendrogeomorphic time series of snow avalanches can yield valuable information for the assessment of recurrence intervals of avalanches on forested paths for which only very limited or no historical data exists, and that this data can be obtained independently from meteorological data or numerical modeling.

1. Introduction

In mountainous regions, snow avalanches are substantial hazards that affect valley slopes, endanger infrastructure or transportation routes and may even cause fatalities (Bründl et al., 2004). In Switzerland, snow avalanches are considered the main natural hazard and have caused 378 fatalities between 1937 and 2015 (Badoux et al., 2016). Avalanche risk management usually involves predetermination of potentially damageable events (Eckert et al., 2008).To this end, it investigates the full set of past avalanche activity on a given path over a long-time period. The aim of this documentation is the realization of hazard maps so as to enforce building restrictions and to design defense structures. To achieve this goal, annual probabilities of occurrence with a given intensity need to be defined for each point of the runout zone

* Corresponding author at: GEOLAB UMR 6042, 4 rue Ledru, 63057 Clermont-Ferrand Cedex 1, France.
E-mail address: adrien.favillier@uca.fr (A. Favillier).

https://doi.org/10.1016/j.coldregions.2018.06.004
Received 27 March 2018; Received in revised form 4 June 2018; Accepted 10 June 2018
Available online 14 June 2018
0165-232X/ © 2018 Elsevier B.V. All rights reserved.

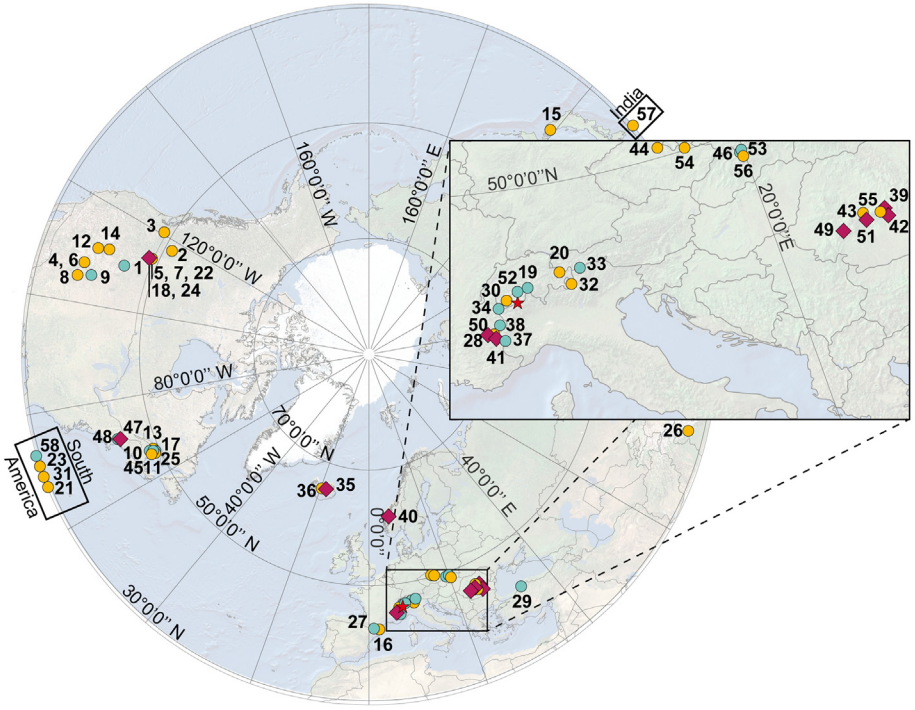

Fig. 1. Synthesis of tree-ring based avalanche reconstructions. Colored dots represent dendrogeomorphic snow avalanche studies with (green) and without (yellow) an estimation of the spatial extent of reconstructed snow avalanche events. Red lozenges represent studies for which avalanche recurrence interval maps have been computed. The red star correspond to the location of this study. **1.** Potter (1969); **2.** Schaerer (1972); **3.** Smith (1973); **4.** Ives et al. (1976); **5.** Butler (1979); **6.** Carrara (1979); **7.** Butler and Malanson (1985); **8.** Bryant et al. (1989); **9.** Rayback (1998); **10.** Larocque et al. (2001); **11.** Boucher et al. (2003); **12.** Hebertson and Jenkins (2003); **13.** Dubé et al. (2004); **14.** Jenkins and Hebertson (2004); **15.** Kajimoto et al. (2004); **16.** Muntán et al. (2004); **17.** Germain et al. (2005); **18.** Pederson et al. (2006); **19.** Stoffel et al. (2006); **20.** Casteller et al. (2007); **21.** Mundo et al. (2007); **22.** Butler and Sawyer (2008); **23.** Casteller et al. (2008); **24.** Reardon et al. (2008); **25.** Germain et al. (2009); **26.** Laxton and Smith (2009); **27.** Muntán et al. (2009); **28.** Corona et al. (2010); **29.** Köse et al. (2010); **30.** Szymczak et al. (2010); **31.** Casteller et al. (2011); **32.** Garavaglia and Pelfini (2011); **33.** Kogelnig-Mayer et al. (2011); **34.** Corona et al. (2012); **35.** Decaulne et al. (2012); **36.** Arbellay et al. (2013); **37.** Corona et al. (2013); **38.** Schläppy et al. (2013); **39.** Voiculescu and Onaca (2013); **40.** Decaulne et al. (2014); **41.** Schläppy et al. (2014); **42.** Voiculescu and Onaca (2014); **43.** Chiroiu et al. (2015); **44.** Tumajer and Treml (2015); **45.** Germain (2016); **46.** Lempa et al. (2016); **47.**Martin and Germain (2016a); **48.** Martin and Germain (2016b); **49.** Pop et al. (2016); **50.** Schläppy et al. (2016); **51.** Voiculescu et al. (2016); **52.** Favillier et al. (2017); **53.** Gadek et al. (2017); **54.**Krause and Křížek (2017); **55.**Pop et al. (2017); **56.**Šilhán and Tichavský (2017); **57.** Ballesteros-Cánovas et al. (2018); **58.**Casteller et al. (2018). (For interpretation of the references to colour in this figure legend, the reader is referred to the web version of this article.)

(Maggioni et al., 2006; Schläppy et al., 2014).

Predetermination is complex as a result of the numerous sources of variability that constrain avalanche activity on a given path (i.e. release area, snow depth, snow quality, path roughness, Eckert et al., 2008). To limit these biases, avalanche specialists first used statistical–topographical or "Norwegian" methods (Lied and Bakkehøi, 1980). These "historical" models assume regional homogeneity in avalanche behavior for a given mountain range, and, to overcome data sparseness at the site-specific scale, pool data from various paths in a common database to derive a simple statistical regression explaining observed runout distances from topographic covariates. The approach was then further developed through the integration of the runout ratio method in which data transformation is applied to fit a probability distribution to standardized observed runout distances (McClung and Lied, 1987; Keylock, 2005). Yet, in alpine countries, where avalanche paths of the same mountain range only rarely exhibit similarity in shape, the fundamental assumption of avalanche homogeneity at the regional scale should be questioned. In addition, a major drawback of this approach is that it depends on the quantity and quality of available data. In many cases, the historical record of run-out distances is not long enough and the resulting fitted probability distribution must be extrapolated to evaluate the run-out distance of avalanche events with long return periods (Ancey and Meunier, 2004).

The Swiss guidelines (Salm et al., 1990) are an alternative to the "Norwegian" method. Here, precipitation data is used to predetermine variations of snow depth for return periods of 30, 100, and 300 years (Salm et al., 1990). The corresponding amount of snow is propagated using the Voellmy (1955) model with tabulated friction coefficient values depending on path geometry and altitude, before the corresponding amount of snow is transformed into a runout distance and velocity profile using a propagation model (Bartelt et al., 1999). One of the main weaknesses of this second family of methods is that the return period of the avalanche is the return period of the corresponding snow depth. The avalanche propagation thus remains a fully deterministic one-to-one link between snow input and runout distance (Eckert et al., 2007). In addition, the number of basic physical processes (snow entrainment or release, turbulent suspension and transformation into an airborne avalanche) occurring in the avalanche course are either unknown or neglected in these models (Meunier and Ancey, 2004). As a consequence, several studies highlighted weaknesses in the values proposed by these guidelines (see e.g. Barbolini et al., 2000), especially due to a significant mismatch in frictional parameter values fitted from field data (Ancey et al., 2004).

Finally, a third option consists in an explicit combination of a propagation model and statistical analysis using Monte Carlo simulations. These statistical-dynamical approaches (Bozhinskiy et al., 2001; Barbolini and Keylock, 2002; Eckert et al., 2008, 2010) use probability distributions as input for the propagation model. Output variable replicates are then used to characterize the return period of snow avalanches. Calibration of statistical-dynamical models with site-specific archival records improves the reliability of the approach considerably (Ancey and Meunier, 2004). A major difficulty is the choice of input distributions that appropriately represent variability of the avalanche phenomenon at the studied site. Data available for calibration typically remains quite limited (Straub and Grêt-Regamey, 2006), non-explicit in nature, and difficult to be implemented in the friction law (Eckert et al., 2010). Models are well capable to simulate contemporary events, corresponding to return period ≤ 30 yr on which they could be calibrated, but uncertainties increase as soon as longer return periods are investigated (Schläppy et al., 2014).

This shortcoming is mainly related to documentation that is only rarely available with satisfying spatial resolution over long timescales and as a continuous record. Historical records are most often biased towards events that caused damage to infrastructure or loss of life and remain largely unavailable for sites that are far away from existing towns (Corona et al., 2012). Any calibration of statistical-dynamical models with archival records has been shown to improve the reliability of the approach considerably (Ancey and Meunier, 2004).

In temperate climate zones, trees serve as silent witnesses of past geomorphic process activity and provide valuable information on event frequencies and spatial patterns of process occurrences (Stoffel and Bollschweiler, 2008). As a consequence, they can theoretically yield valuable information for the assessment of recurrence intervals of avalanches on forested paths with limited or no historical data, and this information can be obtained independently from meteorological data or numerical modeling.

The dating of geomorphic events using tree-ring series, known as dendrogeomorphology (Alestalo, 1971), has been applied repeatedly over the last decades in numerous mountainous regions worldwide to reconstruct multi-decadal to multi-centennial chronologies of snow avalanche events (Fig. 1) and to assess the spatial extent of individual events (see Favillier et al., 2017 for a recent review). With respect to this abundant literature, only twelve studies explore the mapping of return periods of snow avalanche with dendrogeomorphic methods (i.e. Casteller et al., 2011; Corona et al., 2010; Martin and Germain, 2016a; Reardon et al., 2008; Voiculescu and Onaca, 2014, see Fig. 1). In addition, most of the aforementioned studies estimate avalanche return period maps based on the interpolation of the disturbance frequency at the level of individual trees (F) as follows:

$$F_T = (nGDObs_T) \div (A_T) \quad (1)$$

where nGDObs represents the number of growth disturbances related to snow avalanches observed in tree *T*, and A, the total number of years tree *T* was alive. Despite recent efforts to use anisotropic interpolation, that takes account of avalanche flow direction on the slope into account (e.g. Corona et al., 2010), these maps have so far failed to represent the expected patterns of recurrence intervals properly (in the sense that they did not show an increase in recurrence intervals as one moves down the centerline of an avalanche path; e.g. Meunier and Ancey, 2004; Eckert et al., 2007; Schläppy et al., 2014). Specifically, they do not represent the return period of avalanches, but the inverse of the mean frequency of avalanches that could be retrieved locally, which strongly depends on the local characteristics of the forest stand and on the chosen tree-ring methods (sampling strategy, event attribution procedure). As a sole exception, Schläppy et al., 2014, n°41 on Fig. 1), evaluated tree ring based return periods for avalanche runout distances focusing, for each event, on the tree of further reach only. This led a monotonically increasing one-to-one mapping between distance along the path profile and return period, which makes much more sense for potentially affected elements at risk. However, such an approach has never been applied in a 3D mapping frame, yet mandatory for hazard zoning purposes.

In this context, the purpose of this study is to provide a methodology to map tree-ring based recurrence intervals of snow avalanche events. To this end, and based on the procedure proposed by Favillier et al. (2017)–where the noise induced by climate conditions or exogenous disturbances is minimized in tree-ring based process histories–we reconstruct snow avalanche event frequency (1740–2015) of an avalanche slope at Täsch (Canton of Valais, Swiss Alps). In a second step, the temporal accuracy of our reconstruction is checked through a comparison with the historical documentation available at our study sites. Finally, an expert delineation of the spatial extent of past events is used, and recurrence interval maps are derived from their distribution and confronted to the interpolations of the frequency of growth disturbances commonly used in the literature.

2. Study site

The site under investigation (46°3′N, 7°46′E, 307.6 ha, 1450–3247 m asl) is located on the west-facing slope of the upper Zermatt valley in the Swiss Alps (Canton of Valais, Switzerland, Fig. 2a). Its geology is dominated by gneisses with amphibolite zones oriented NE-SW (Federal Office of Topography Swisstopo). Snow avalanches are commonly naturally triggered from several non-forested release zones located between 2200 and 3500 m asl. Once released, they pass through a forested slope mainly composed of European larch (*Larix decidua* Mill.). At the bottom of the slope, the avalanche track crosses the road from Täsch to Zermatt during winter (Fig. 2b). As a consequence, 10-m high deflecting dams and a tunnel were built in the 1990s to protect properties and infrastructures from snow avalanches.

In detail, three main paths have been identified at our study site (Fig. 2b):

(i) In the northernmost path T1 (60.6 ha), snow avalanches are released from a steep area (> 35°) located between 2250 and 2700 m asl. The couloir, poorly incised, is characterized by steep slopes (25°-35°) between 1500 and 2300 m asl. The runout zone (< 10°) is limited to the valley floor located below 1500 m asl.
(ii) The slope angle of T2 (87.8 ha) decreases progressively from > 35° in the release area to 15–20° below 1700 m asl and < 10° next to the Mattervispa (1500 m asl). In its upper part, this track has three steep, incised rocky channels converging at ~1800 m asl with the Täschwang couloir. At this path, preliminary analysis of orthophotos highlights that the forest stand has repeatedly suffered from severe damage and deflecting barriers are installed along the left side of this channel (1750–2500 m asl) to protect Zermettjen and the access road to Zermatt (Fig. 2) since at least 1941.
(iii) T3 (61 ha) is characterized by a complex release area divided into two units that are separated by a 150-m high rockwall at 2500 m asl. Below 2200 m asl, the forested slope is incised by several channels converging with the Täschwang couloir at 1650 m asl.

According to the nearby weather station of Zermatt (46°3′N, 7°75′E, 1638 m asl), annual temperature in the Zermatt valley is 4.2 °C for the period 1981–2010 and average annual precipitation amounts to 639 mm. During winter, mean air temperature (DJF) is −3.7 °C while precipitation amounts to 125 mm. From November to April, precipitation falls primarily as snow and average annual snowfall reaches 270.2 cm for the period 1982–2010 with an average of 39 days of snow per year. Finally, there are no indications in the historical archives nor in the local authority testimonies of any debris flow activity that could significantly affect the studied forested stand.

3. Material and methods

3.1. Compilation of historical archives

Several documentary sources were used in this study to compile a precise and as complete as possible historical chronology of snow avalanches in the Täschwang paths. Data were extracted from local newspapers, ecclesiastical archives and stakeholder chronicles. In total, 6 regional and local newspapers (i.e. Confédéré, Walliser Bote, Le Nouvelliste, Journal et Feuille d'avis du Valais, Le Rhône, La Sentinelle), published between September 1861 and June 2014, were examined via the Swiss virtual newspaper archives available online at http://newspaper.archives.rero.ch/Olive/ using keywords such as “Täschwang” corresponding to the toponymy of the main paths. In addition, “Täsch” and “Zermatt” were used as keywords, as they refer to the two closest localities as well as “avalanche” and “Lawine”, the French and German words for snow avalanche. In addition, the annual winter reports published by the Institute for Snow and Avalanche Research (Institut für Schnee und Lawinenforschung–SLF) since 1935 and local chronicles available at the Institut zur Erforschung der Geschichte des Alpenraums (FGA) and from the Swiss-scale database from Laternser and Pfister (1997) were reviewed in detail. Finally, in order to complement this archival database, five aerial flight campaigns – available from the Federal Office of Topography (Swisstopo; 1:20,000) –and the Siegfried map (Mischabel, 533, edition 1909) were compared to detect potential damaging avalanches and to reconstruct forest dynamics since 1941.

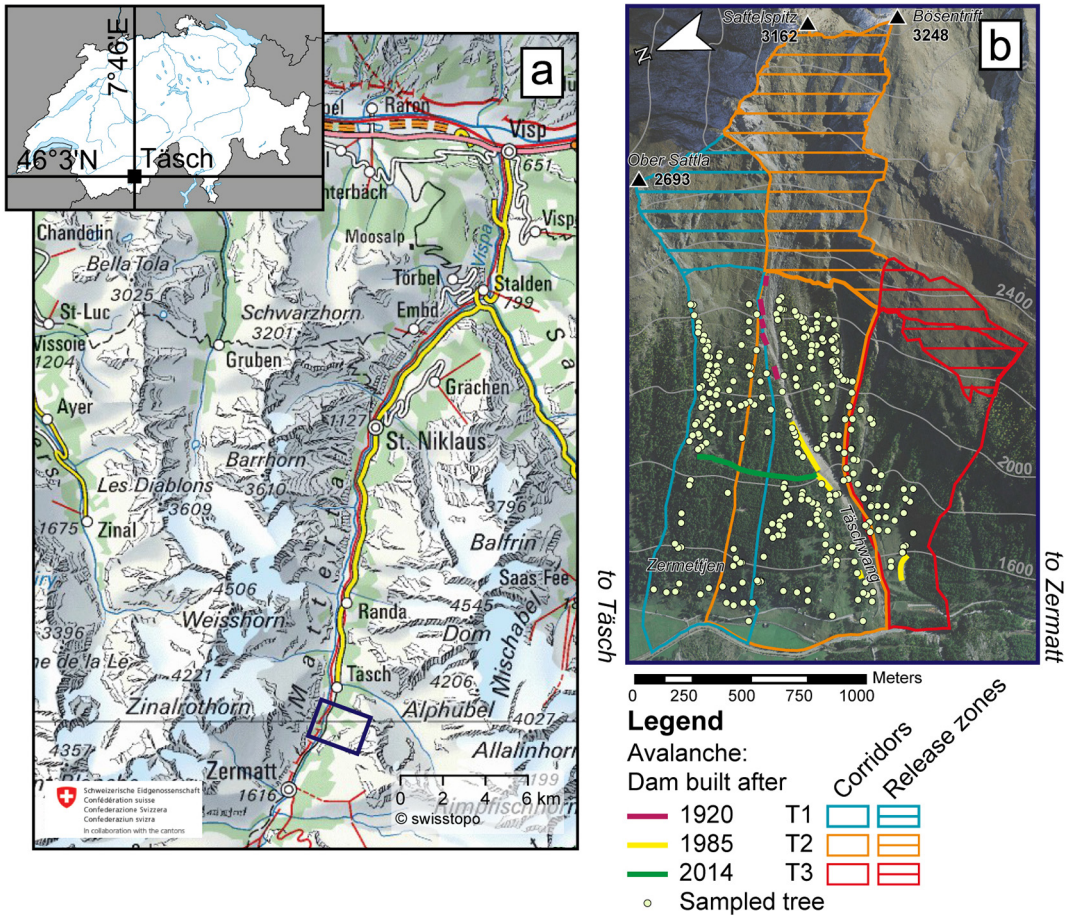

Fig. 2. Location of the study site: (a) the Zermatt valley in the canton of Valais, Switzerland, (b) Spatial distribution of the sampled trees within the three paths and their release areas. The green lines represent the avalanche dams built after major avalanche events. Map and aerial photography are reproduced by permission of swisstopo (BA18022). (For interpretation of the references to colour in this figure legend, the reader is referred to the web version of this article.)

3.2. Sampling strategy, identification, dating and classification of growth disturbances

To reconstruct past avalanche activity based on dendrogeomorphic techniques, a total of 620 increment cores and 60 cross-sections have been sampled from 307 European larch (*Larix decidua* Mill.) trees using a Pressler increment borer (diameter 5.15 mm, maximum length 40 cm) in autumn 2015. A minimum of two cores was extracted per tree, one upslope and one in the downslope direction (Stoffel and Bollschweiler, 2008). Additional data were collected for each tree including its diameter at breast height, description of the disturbance (i.e. amount of scars, decapitation, tilting), and exact position of the sampled tree using a 1-m precision GPS device.

Trees presenting obvious evidence of snow avalanches, such as decapitation, tilting, and injury, were preferentially selected. Following recent recommendations by Stoffel and Corona (2014), old trees were selected to extend the reconstruction of past avalanche events as far as possible. Nevertheless, younger trees were also considered to account for the loss of sensitivity of older trees in recording mass-movement signals (Šilhán and Stoffel, 2015). Sampling height was chosen according to the morphology of the stem: (i) injured trees were sampled at the height of the disturbance from the overgrowing scar tissue; (ii) tilted trees were analyzed at the maximum bending angle (Stoffel et al., 2013); and (iii) cross-sections and cores from decapitated trees were taken at the lowest possible position on the tree to maximize the number of available rings (Stoffel and Bollschweiler, 2008). Samples were prepared and data processed following standard procedures described in Stoffel et al. (2013). Growth disturbances (GD) such as injuries –i.e. impact scars– and callus tissues (CT) (Stoffel et al., 2010), tangential rows of traumatic resin ducts (TRD) (Schneuwly et al., 2008, 2009), compression wood (CW) and abrupt growth suppression (GS; Kogelnig-Mayer et al., 2013) were identified in the tree-ring series and cross-dated against two local reference chronologies (Büntgen et al., 2005), so as to correct our series for possibly missing and false rings.

Intensities were then assigned to each GD using criteria defined by Kogelnig-Mayer et al. (2011). This step was included to emphasize features which were clearly associated with avalanche activity. Intensities of growth suppression, compression wood and TRDs were classified according to Schneuwly et al. (2008) and Frazer (1985) to distinguish between weak (intensity class 1), medium (intensity class 2), and strong (intensity class 3) reactions and clear evidence of injuries (intensity class 4).

3.3. Detection of past avalanche events in growth disturbance series

To detect past snow avalanche events – which correspond to the occurrence of one snow avalanche at least in the selected path at a yearly resolution – in the GD series, we adopted the four-step procedure described in Favillier et al. (2017) that underlines the necessity to disentangle the potential effects of snow avalanches from disturbance pulses caused by climatic or exogenous factors, such as cold/dry years or larch budmoth outbreaks:

(i) In a first step, for each year t with a minimum of 15 trees available in each path, an index I was calculated, according to Shroder (1978) and based on the percentage of trees showing responses in their tree-

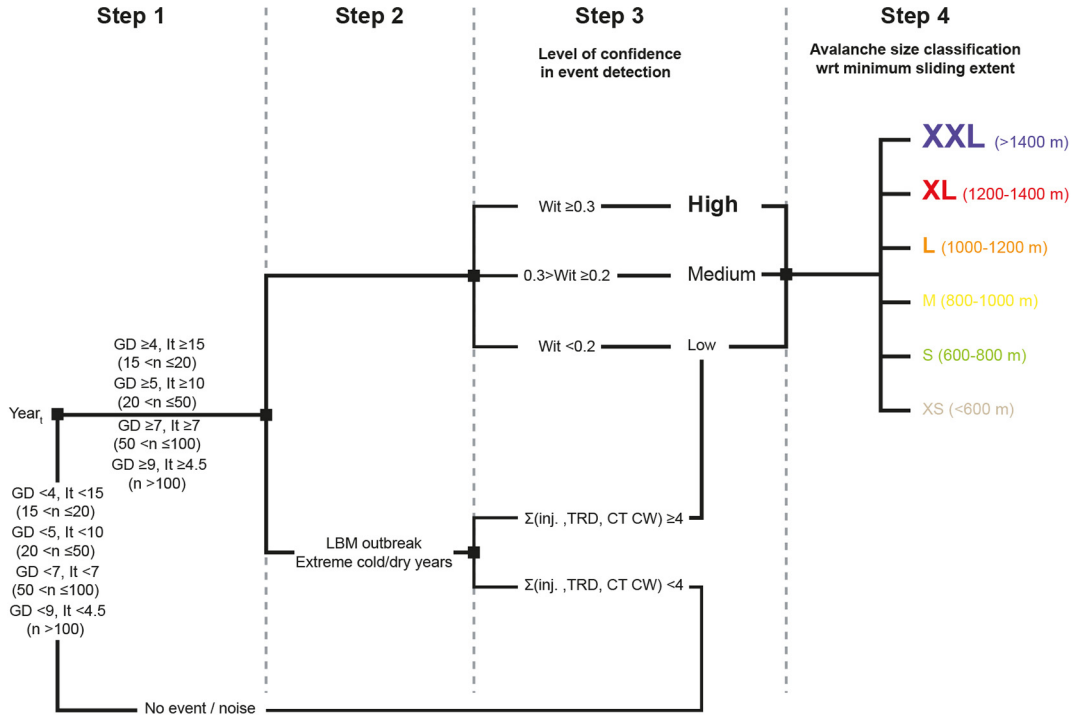

Fig. 3. Synoptic diagram of the 4-step approach used for the detection of avalanche events in tree-ring series, adapted from Favillier et al. (2017).

ring record in relation to the number of sampled trees being alive in year t:

$$I_t = \left(\left(\sum_{i=1}^{n} R_t\right)/\left(\sum_{i=1}^{n} A_t\right)\right) * 100 \quad (2)$$

where ΣR represent the number of trees responding to an event in year *t*, and ΣA is the number of trees alive in year *t*. Following recommendations from Butler and Sawyer (2008), a double threshold for sample sizes of 15–20 (GD > 4 and *It* > 15%), 21–50 (GD > 5 and *It* > 10%), 51–100 (GD > 7 and *It* > 7%), and ≥ 100 trees (GD > 9 and *It* > 4.5%) has been used to discriminate potential avalanche and non-avalanche events in accordance with statistically determined threshold as defined by Corona et al. (2012). These thresholds also aimed at limiting the inclusion of noise related to snow creeping (Stoffel and Corona, 2014), snow loading (Martin and Germain, 2016a), or any other kind of ecological disturbances (Butler and Sawyer, 2008; Corona et al., 2012) in the process reconstruction (Fig. 3).

(ii) The grey larch budmoth (LBM, *Zeiraphera diniana* Gn.) is a foliage feeding Lepidopteran insect responsible for periodical outbreaks (8- to 10-year intervals), mainly in the interior valleys of the European Alps (Baltensweiler et al., 1977). The feeding of LBM on larch needles causes massive defoliation that results in growth suppression in trees lasting for 3–4 years (Kress et al., 2009) which may, thus, interfere with the dendrogeomorphic signal contained in tree-ring series. In total, 26 triplets of LBM outbreak years (i.e. three consecutive years, see Table 1) have been reconstructed in the Swiss Alps since 1740 CE according to Esper et al. (2007) and Büntgen et al. (2009). Similarly, climate extremes such as cold summers and prolonged droughts are susceptible to lastingly affect larch growth (Battipaglia et al., 2010; Lévesque et al., 2013; George et al., 2017) and to cause prolonged growth suppressions that may be confound with avalanche-induced GDs. According to Battipaglia et al. (2010), extremely cold summers were reconstructed in the central Alps from tree-ring data and historical archives in 1740, 1742, 1767, 1769, 1814, 1816, 1829, 1833, 1851, 1860, 1896, 1912, 1924, 1964, 1972, 1984, and 1995. Based on the gridded HISTALP point temperature information (Efthymiadis et al., 2006) closest to the study site, 11 years with negative May–September anomalies of temperature – 1.5 SD below the average – could be found for the period 1780–2008 and have thus been considered as cold summers years (Table 1). In the same way, eight years with negative April–July precipitation anomalies (i.e. -1.5 SD) were identified in the HISTALP point precipitation database for the period 1800–2003 (Efthymiadis et al., 2006). These years have been considered as drought years.

Table 1
Larch budmoth events (according to Esper et al., 2007 and Büntgen et al., 2009), as well as extremely cold and dry summers (Battipaglia et al., 2010; Efthymiadis et al., 2006) in the Swiss Alps. All these years have been carefully analyzed due to probable interferences between snow avalanche damage in trees, as well as LBM and climatic signals that may induce comparable growth reduction in tree-ring series.

2003	**1945**	*1903*	*1851*	**1792**
1995	**1937**	**1896**	*1843*	**1779**
1984	*1932*	*1896*	**1838**	**1771**
1981	**1931**	1893	*1833*	*1769*
1980	*1924*	1892	**1830**	*1767*
1979	**1923**	**1888**	*1829*	**1758**
1978	1921	**1880**	**1821**	**1753**
1972	*1919*	*1879*	*1821*	**1743**
1972	**1915**	1870	*1817*	*1742*
1965	*1912*	1865	*1816*	*1740*
1963	1911	**1864**	*1814*	
1962	*1910*	*1860*	**1811**	
1954	**1908**	**1856**	**1801**	

LBM-outbreak years, *Extreme cold summer*, Drought years.

Potential avalanche events detected in step 1 that coincided with LBM outbreak episodes or extremely cold/dry years were therefore examined in more detail. To limit possible interferences between geomorphic, climatic, and LBM signals, growth suppressions were systematically excluded from the account of GDs and a minimum threshold

of 4 GDs was retained to discriminate avalanche from non-avalanche events (Fig. 3).

(iii) In a third step, the type and intensity of GDs were used to evaluate a qualitative level of confidence associated to the detection of each reconstructed event. To this end, a weighted index factor (W_{it}) adapted from Kogelnig-Mayer et al. (2011) was computed for each avalanche event detected in step 1 as follows:

$$W_{it} = \frac{[(\sum_{i=1}^{n} T_i*7) + (\sum_{i=1}^{n} T_s*5) + (\sum_{i=1}^{n} T_m*3) + (\sum_{i=1}^{n} T_w*1)]}{\sum_{i=1}^{n} A_t} \quad (3)$$

where, for each year t, T_i represents the sum of trees with injuries; T_s represents the sum of trees with strong GDs; T_m represents the sum of trees with medium-intensity GDs; T_w represents the sum of trees with weak-intensity GDs, and where A gives the total number of trees alive in year t. Based on the W_{it}, we then distinguish between low (LLC, $W_{it} < 0.2$), medium (MLC, $0.3 > W_{it} > 0.2$), and high (HLC, $W_{it} > 0.3$) levels of confidence in the reconstruction and attributed this evaluation to the avalanche event detection. In addition, and despite the precautions taken at each of the previous step, each event detected at step 2 was only rated with a LLC (Fig. 3).

(iv) Finally, avalanche events and corresponding GDs were mapped using the ArcGis 10.2 Time Slider (Kennedy, 2013; ESRI, 2013) to estimate the minimum sliding extent (ME, w.r.t the barycenter of the avalanche release zones) of each avalanche event. On the basis of ME, avalanche events with ME < 600 m, 600 m < ME < 800 m, 800 m < ME < 1000 m, 1000 m < ME < 1200 m, 1200 m < ME < 1400 m, and ME > 1400 m were classified as eXtra Small (XS), Small (S), Medium (M), Large (L), eXtra-Large (XL) or eXtra-eXtra-Large (XXL) events, respectively.

The age structure of the stand was approximated by counting the number of tree rings of sampled trees and was visualized after interpolation. However, and because trees were not sampled at their stem base and the piths as well as the innermost rings of some trees were rotten, the age structure is biased and does not reflect inception or germination dates. Nonetheless, it may provide valuable insights into major disturbance events at the study site with reasonable precision, as *L. decidua* has been shown repeatedly to recolonize surfaces cleared by snow avalanches or other mass-movement processes in the years following an event (Stoffel et al., 2006; Van Der Burght et al., 2012).

3.4. Computation of avalanche events recurrence interval maps

In total, three recurrence interval maps (Rims) were computed at our study site. In Rim1, the individual impact interval for each tree (F_T) was calculated according to Eq. (1), following the interpolation method previously used by Reardon et al. (2008), Corona et al. (2010), Decaulne et al. (2012), or Martin and Germain (2016a). Rim1 was then visualized in ArcGIS 10.2 (ESRI, 2013). To estimate realistic values for the impact interval of events in areas where it could not be determined with dendrogeomorphic methods (Dale and Fortin, 2014), we spatially interpolated individual recurrence intervals using an inverse distance weighted interpolation algorithm. To ensure spatial robustness, interpolations were performed with an ellipse-shaped search (major axis: 280-m; minor axis: 96-m) where the anisotropy was set using an angle of 280° due to the presence of a strong directional influence (i.e. points are strongly related to those upslope of their location). Between ten and twenty-five neighbors were included within the eight sectors.

Rim1 relies on trees considered as proxies for past avalanche events. Yet, it does not account for the nature nor the physic of snow avalanches, classified as fast-moving mass-movements (McClung and Schaerer, 2006) that may have a huge destructive power reinforced by transported debris (Bründl et al., 2010) and potentially affect every tree within their paths.

To limit this bias, Rims2–3 were computed with a three-step procedure. In a first step, we (i) delineated the minimum area affected by each reconstructed event based on the spatial pattern of impacted trees, the geomorphology of the slope and the flowing nature of the process under investigation. We (ii) calculated recurrence intervals at each point of the slope as the ratio between the total number of years included in the dendrogeomorphic reconstruction and the number of times the snow avalanches reached this point. Finally, we (iii) built Rims2–3 without applying an interpolation procedure. Rim2 differs from Rim3 by the total number of years (275 and 75 years, respectively) included in the dendrogeomorphic reconstruction. Provided a precise (i) estimation of the number of avalanche events and (ii) delineation of past events, this procedure enables an approximation of recurrence intervals of snow avalanches at each pixel of the paths, and independently from individual tree ages.

4. Results

4.1. Snow avalanches recorded in historical archives

Analysis of historical archives yielded data on 45 snow avalanches (32 avalanche years) in the vicinity of Täsch during the 20th century. In total, 24 (16 avalanche years) out of the 45 snow avalanches occurred at the Täschwang site. Within these avalanches, four were observed during the first half of the 20th century in 1907, 1914, 1919, and 1920. By contrast, 17 occurred during the period 1950–2000 in 1962, 1974, 1975 (4 events), 1977 (3 avalanches), 1978, 1979, 1980, 1981, 1983 (2 avalanches), and 1985 (2 avalanches). Finally, 3 avalanches were documented during the early 21st century in 2012, 2013, and 2014. According to the analysis of archival documents, avalanches occurred preferentially from January to April (75.5%) and at the beginning of June (4.4%).

Three high-magnitude avalanches are precisely described in historical documentation (1920, 1984 and 2014). According to the Walliser Bote newspaper, an extreme snow avalanche occurred on January 17, 1920. This avalanche did not follow the classical path; by contrast, it reached “Zermettjen” – a locality 780 m downslope of the usual avalanche deposit where it destroyed a huge part of the forest, burying a barn with a 9-m thick snow tongue and killing 18 cattle (Fig. 4a). In 1984, another avalanche reached the Mattervispa River and killed 11 persons in cars on the road linking Täsch to Zermatt. On March 4, 2014, several newspapers report a snow avalanche – with a volume of approximatively 80,000 m^3, comparable to the 1984 event – that buried the road to Zermatt and filled the northern entrance of the avalanche protection tunnel built after the 1984 event (Fig. 4b).

4.2. Age structure of the stand

In total, 307 European larch (*Larix decidua* Mill.) trees were sampled with 620 increment cores and 60 cross-sections. In total, 108, 180, and 45 trees were sampled on tracks T1, T2 and T3, respectively. After cross-dating, data on the pith age at breast height indicates that European larch trees growing at Täschwang were on average 145 yrs. old ($\sigma \pm 98$ yrs). The oldest tree selected for analysis reached breast height in 1617 CE while the youngest tree only attained sampling height in 2011. As illustrated in Fig. 5, the stand is dominated by 10–100-yr (46.3%) and 200–300-yr (30.0%) old trees, whereas 100–200-yr old trees only represent 16.9%. In total, 14 trees could be found with ages exceeding 300 years.

The comparison of aerial photographs and maps for the period 1909–2016 (Fig. 6) shows significant variations in the extent of the forest stand. In 1909, the uppermost trees were located at 2300–2400 m asl at T2 and reached 2000 m asl at T1. In 2016, this position has considerably evolved and the current timberline is above 2300 m asl at both paths. At T1, the diachronic analysis reveals (i) the destruction of a

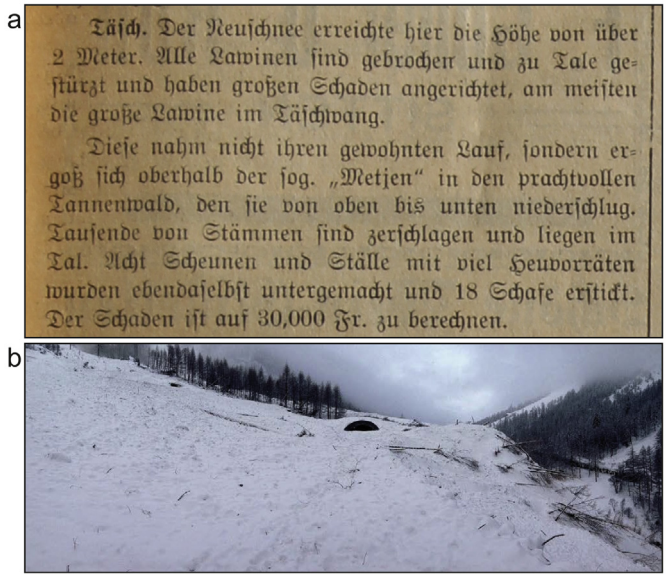

Fig. 4. (a) Description of the avalanche of January 1920 in the Walliser Bote published 17th of January 1920. English translation: "*Täsch: The new snow at the locality exceeded 2 meters. All avalanche couloirs produced events to rush down to the valley where they caused large damage, especially in the case of the large Täschwang avalanche. The avalanche did not follow its usual trajectory, but left its couloir above the so-called "Metjen" from where it descended into a wonderful conifer forest to destroy it all the way down to the valley floor. Thousands of stems have been broken and are now accumulated in the valley. Eight stables and barns with plenty of hay reserves have been devastated and 18 sheep have been killed. Damage has to be estimated in the order of 30,000 francs*", (b) The snow avalanche ($\approx$80,000 m^3) of March 4, 2014 buried the northern entrance of the avalanche protection tunnel and the road linking Täsch to Zermatt (Feistl et al., 2015), picture extracted from Techel et al. (2015).

400 × 800 m strip of forest, located in the central parts of T1 and T2, between 1909 and 1941; (ii) a reforestation of this area between 1941 and 1977; and (iii) only a slight reshaping of the forest limits between 1977 and 2016. Coupling the diachronic analysis to both historical archives and the age structure of the stand lead us to hypothesize that approximately 32 ha of forest were destroyed by the high-magnitude snow avalanche of January 1920 and that this surface has been re-colonized ever since.

4.3. Distribution of growth disturbances and chronology of avalanche events

Sampled cores and cross-sections allowed identification of 2570 GD in the tree-ring series for the period 1740–2015, 799 of which were considered strong avalanche indicators (Classes 3 or 4). Table 2 summarizes the types of GD as well as their intensity. TRDs (49.4%), CT (3.1%), and CW (2.6%) were the GDs most frequently (55.1%) identified in the samples, followed by growth suppressions (GS; 38.7%). By contrast, only 164 injuries were sampled, which represents 6.4% of the dated disturbances. In total, 35.4% of the GDs were rated as intensity 2 and 33.5% as intensity 1. Intensities 3 and 4 represent 24.7% and 6.4% of all detected GDs, respectively. The oldest GD identified in the tree-ring series was dated to 1659 CE. GDs are more frequent after 1900 and nearly every year exhibited GD in a small number of trees.

On the basis of our 4-step-procedure (Fig. 3, 7), tree-ring analyses allowed identification of 51 years with evidences of snow avalanche in at least one path between 1740 and 2013 (Fig. 7). The oldest event was recorded in 1741 (T2), the most recent event in 2013 (T1-T2-T3).

In total, 31 (1740–2015), 35 (1740–2015), and 5 (1772–2015) avalanche events were reconstructed at sites T1, T2, and T3, respectively. Based on possible interferences between avalanche activity, climatic, and LBM signals in the tree-ring series (step 2), and on the

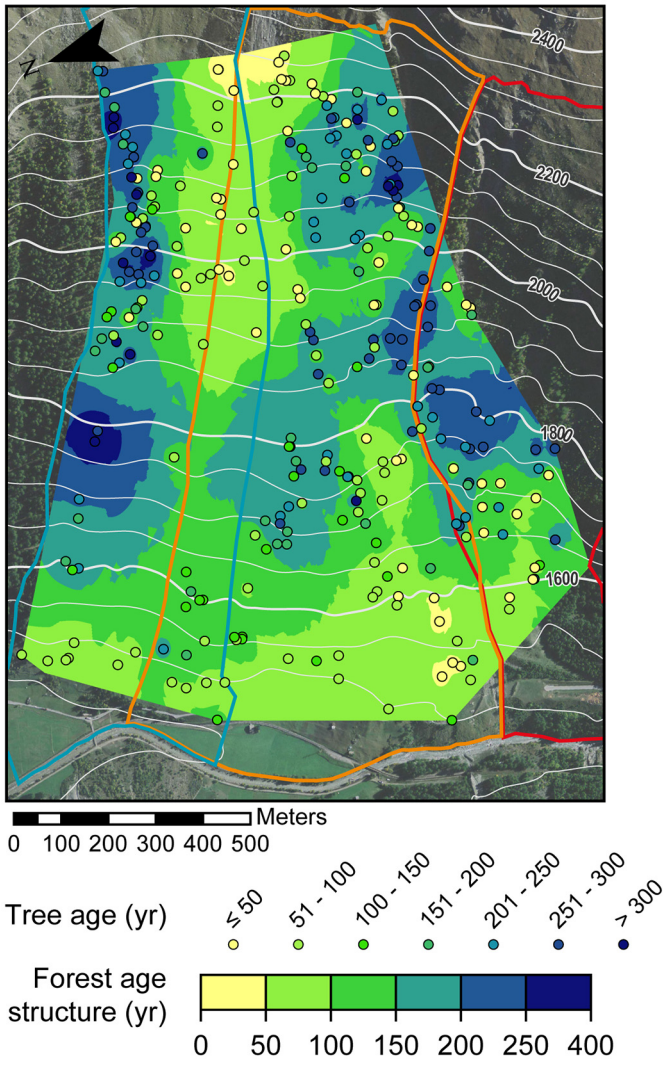

Fig. 5. Age structure of the forest stand growing at the Täschwang sites and its avalanche paths.

basis of the Weighted Index Factor (W_{it}; step 3, Figs. 7, 8) that accounts simultaneously for the type and intensities of GDs, we assigned high and medium levels of confidence to 32 and 12 events, respectively. By comparison, 27 events with a Wit < 0.2, and characterized by a majority of weak and medium GDs, were therefore reconstructed with a LLC. Amongst the 42 potential events that coincide with LBM outbreak episodes or extreme climatic years, 24 were excluded from the reconstruction and 18 were rated with a LLC (Fig. 7, 8).

Higher levels of confidence were assigned to events that occurred in T1 (16 HLC and 4 MLC events) and T2 (11 HLC and 8 MLC events). Tree-ring signatures related to past snow avalanche activity were, by contrast, less frequent at T3 but all events were considered to have a HLC. For the period covered by historical archives, 9 (43.8%) out of the 16 avalanche years documented in historical archives were reconstructed with tree-ring records in T2 (1920, 1975, 1977, 1978, 1983, 2012 and 2013) and T1 (1962, 1975, 1977, 1978, 1981, 2013). By contrast, an insufficient number of GDs and/or possible interferences with LBM outbreaks and climatic extremes prevented us from retrieving the documented snow avalanches that occurred during winters 1907/08, 1918/19, 1961/62, 1973/74, 1978/79, 1979/80, 1980/81, 1984/85 and 2014/15.

Considering all reconstructed events within the study area, the mean event recurrence interval for the Täschwang avalanche paths is 3.8 years (or 2.6 events per decade) for the period 1740–2015.

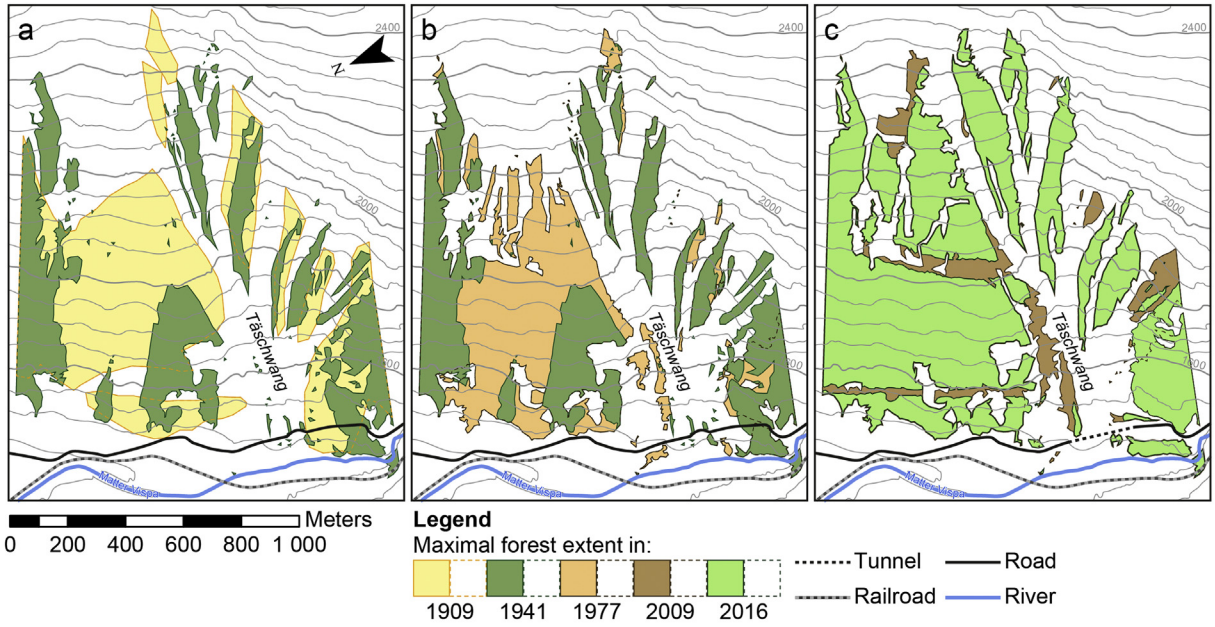

Fig. 6. Diachronic evolution of the forest stand at Täschwang for the period 1909–2016: (a) 1909–1941, (b) 1941–1977, and (c) 2009–2016.

Table 2
Intensity of reactions and types of growth disturbances (GD) assessed in the 307 larch trees selected for analysis.

Type/ intensity	1	2	3	4	Total
Injuries	–	–	–	164 (6.4%)	164 (6.4%)
CT, TRD, CW	572 (22.3%)	403 (15.7%)	441 (17.2%)	–	1416 (55.1%)
GS	289 (11.2%)	507 (19.7%)	194 (7.5%)	–	990 (38.5%)
Total	861 (33.5%)	910 (35.4%)	635 (24.7%)	164 (6.4%)	2570 (100%)

Avalanche event frequency is not, however, constant over time but shows a clear increase from one event per decade for the period 1740–1960 (22 events) to 8.9 events.decade^{-1} between 1961 and 2015 (49 events). Maximum decadal frequencies are systematically observed in the recent past, from 1971 to 1980 (9 events), 1981–1990 (8 events), and 2001–2010 (13 events). Conversely, no events could be reconstructed for the periods 1742–1795, 1804–1860, 1880–1899 and 1904–1918.

In details, at the level of individual paths, the highest avalanche activity was observed at T2 (35 events, 11 rated HLC, 8 MLC, mean recurrence interval 7.9 yr) and T1 (31 events, 16 rated HLC, 4 MLC, mean recurrence interval 8.9 yr). Conversely, T3 is characterized by lower activity (5 HLC events).

4.4. Spatial extent of avalanche events and recurrence interval maps

The spatial distribution of trees with GDs in a specific year has been used to estimate the minimum sliding extent (MSE) for each reconstructed avalanche. In total, 51 out of the 71 (71.8%) reconstructed events exceeded a length of 1200 m and were thus classified as XL (5) or XXL (46) snow avalanches (Fig. 9). The remaining 20 events were classified as L (8) or M (12) avalanches. There is no particular pattern between MSE and LBM outbreak or drought years. During these years, 11 out of 18 avalanche events were rated as XXL, 3 as M-sized and 2 as L-sized. Moreover, no clear relation was observed between the size of the event and the level of confidence associated to its reconstruction. By way of example, amongst the 46 XXL events, 20 were considered with a LLC. On the contrary, amongst the 32 events considered with a HLC, 16 events were reconstructed as extreme (XXL), five exceeded 1200 m in length (XL, 1796-T2, 1968-T1, 1996-T1, 2007-T3 and 2014-T1) and only eight were of limited extend.

The first recurrence interval map (Rim1, Fig.10a) was computed from recurrence intervals as obtained for individual trees (eq. 1) and by using an inverse distance weighted interpolation. Highest recurrence intervals (13–18 yr) are observed in the release areas of T1 and T2, above 2200 m asl and at the lowermost parts of the Täschwang channel whereas lower recurrence intervals (60–100 yr) are computed in the central part of the channel between 1650 and 2100 m asl. Conversely, highest recurrence intervals, derived from tree-ring analysis, exceed 150 years in the northern part of T1 and at the southern edge of T2. In addition, clear “bulls eye” effects – related to the inverse distance weighting – can be observed e.g. at 1800 m asl on the northern part of T1 or at 1650 m asl in the southern margin of T3.

In Rim2 (Fig. 10b), our expert approach was used to delineate the spatial extent of each reconstructed event based on the position of disturbed trees, geomorphology of the slope and flow patterns of snow avalanches at the site. Rim2 results from the superimposition of all reconstructed extents and thus represents the average interval of time that elapses between events reaching a given location for the period 1740–2015. The spatial pattern of Rim2 obviously differs from Rim1: within T1 and T2, the recurrence intervals increased rapidly with distance downslope. Return periods range from 10 to 11 years at the release area of T1 (1900–2200-m asl) and T2 (2150–2400-m asl) and exceed 150–275 years on the interfluve between both paths (1500–1750-m asl). In addition, the Täschwang channel, characterized by < 10 yr recurrence intervals is clearly delineated in Rim2 (whereas it remained invisible in Rim1). To account for the strong non-stationarity of the dendrogeomorphic reconstruction characterized by an obvious increase in avalanche recurrence intervals since the 1960s, Rim3 was also computed for the period 1961–2015 (Fig. 10c). Rim3 evidences recurrence intervals (i) < 6 yr in the release areas of T1 and T2 and in the Täschwang channel and (ii) > 18 yr in the lowermost part of both path below 1600 m asl. No information is available for the lowermost part of the forested strip, destroyed by the event of 1920, as no clear evidence of avalanche activity could be found in this sector since the 1960s.

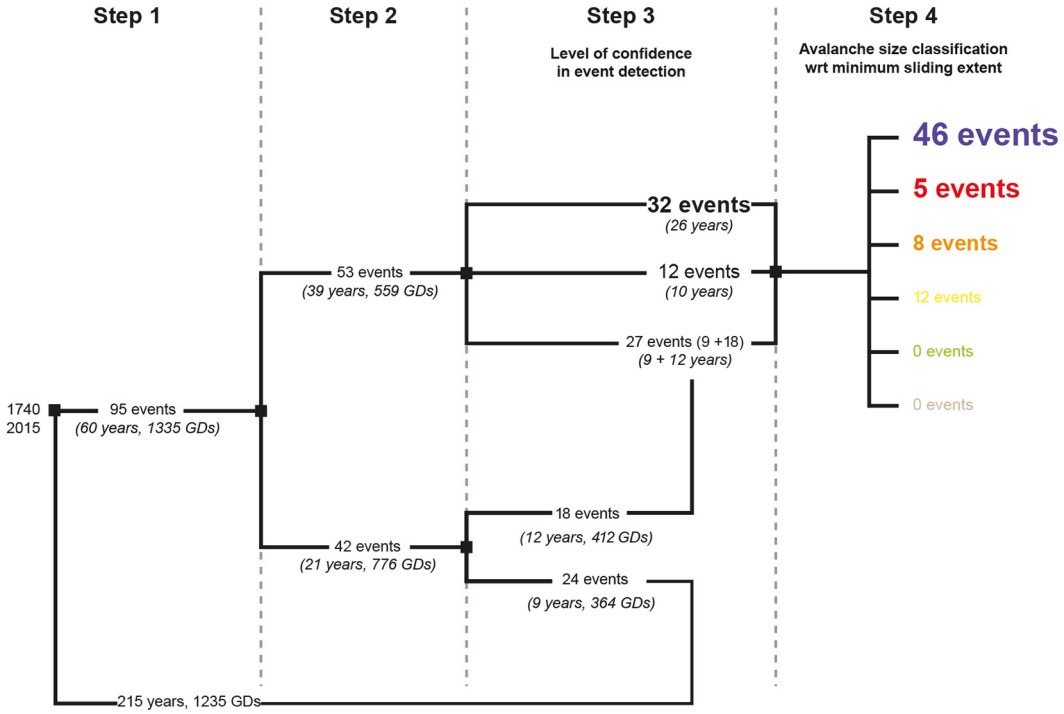

Fig. 7. Simplified synoptic diagram showing the characteristics (possible interference with climate or larch budmoth outbreaks, level of confidence, and minimum slide extent) of the reconstructed events.

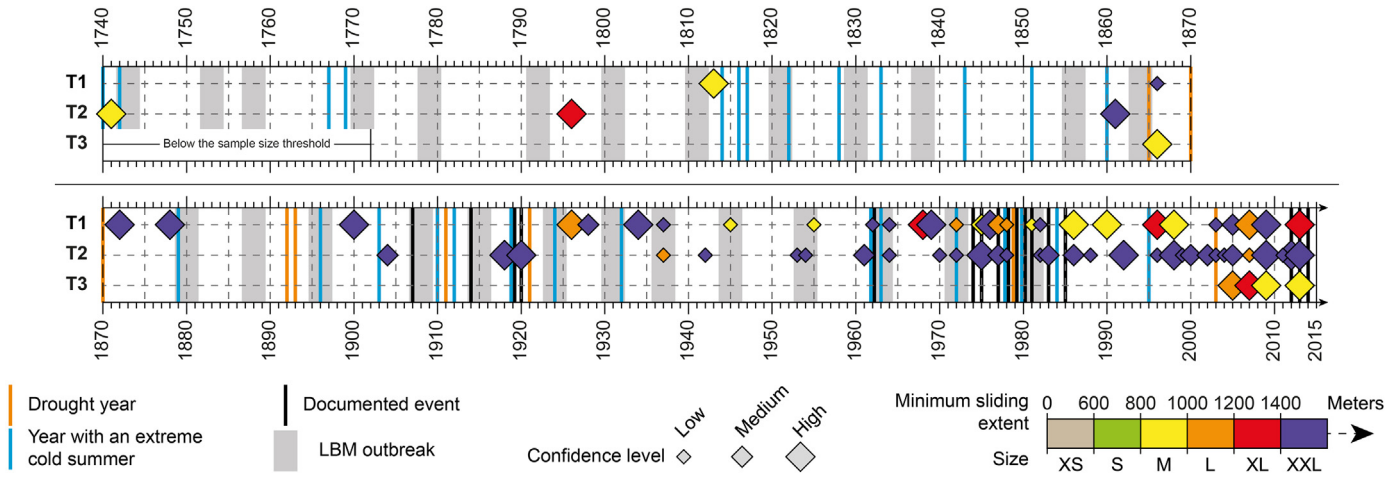

Fig. 8. Avalanche events reconstructed for the period 1740–2015 in avalanche paths T1, T2, and T3. Symbol sizes are proportional to the level of confidence, whereas the colour range denotes the minimum slide extent. Grey bands represent triplets of years associated to LBM outbreaks. Vertical lines show snow avalanche events documented in historical archives (black), as well as extremely dry (orange) and cold (blue) summers. (For interpretation of the references to colour in this figure legend, the reader is referred to the web version of this article.)

5. Discussion

5.1. Spatio-temporal accuracy of the reconstruction

The study we report here employs dendrogeomorphic techniques on three avalanche paths at Täschwang with the aim to assess recurrence interval maps of past avalanche activity. Specifically, we focus on events defined as the area affected a given winter by one or several snow avalanches in a given path. To meet this objective, the detection procedure developed by Favillier et al. (2017) was used (i) to disentangle geomorphic signals in tree-ring series (related to the occurrence of snow avalanches) from signals induced by other external disturbances and (ii) to estimate the robustness of our tree-ring based snow avalanche reconstruction. Based on this procedure, 71 snow avalanche events were reconstructed in 51 different avalanche years. The reconstruction therefore complemented the historical chronology significantly as the first “only” yielded data on 24 snow avalanche events for 16 different winters between 1907 and 2014, and by extending the series back to 1740 CE. In total, 9 out of 16 (56.3%) avalanche years listed in historical documents were retrieved with the dendrogeomorphic approach, namely in 1920 (T2), 1962 (T1), 1975 (T1, T2), 1977 (T1, T2), 1978 (T1, T2), 1981 (T1), 1983 (T2), 2012 (T2), and 2013 (T1, T2, T3).

This success rate is comparable to previous tree-ring reconstructions performed both in the French (Corona et al., 2010, 2012; Schläppy et al., 2013) and the Swiss Alps (Favillier et al., 2017) but highlights, at the same time, some limitations in our approach in providing a complete picture of avalanche activity at a site. These limitations are related

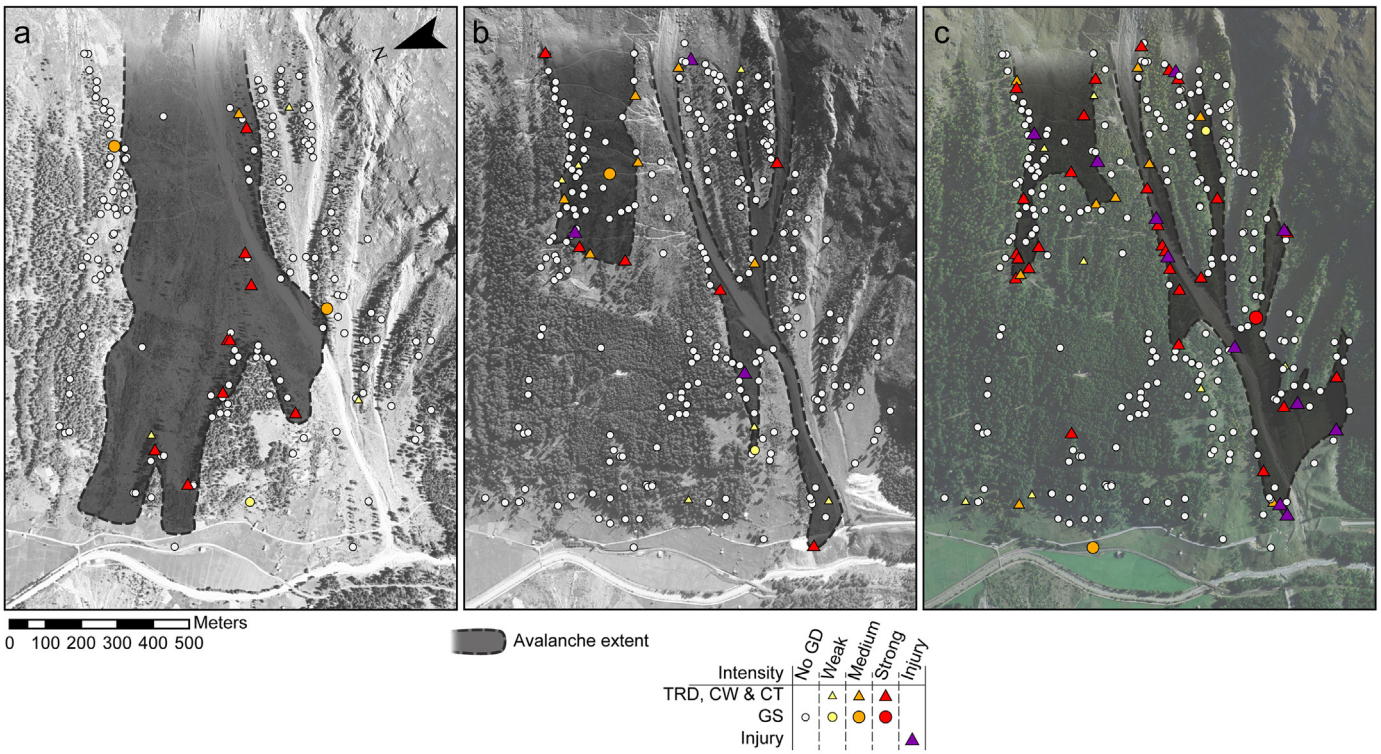

Fig. 9. Reconstructed Minimum Sliding Extent (MSE) of avalanches that occurred (a) on January 16, 1920, at T1 (b) in 1986, at T1 and T2, and (c) in 2009, at T1, T2 and T3, as derived from the location of disturbed trees and interpretation of the aerial pictures taken in 1941, 1988 and 2009 (in the background, aerial photographs are reproduced by permission of swisstopo, BA18022).

to (i) the energy of snow avalanches that have to be of sufficient magnitude to have impacts on trees; (ii) major avalanches that destroyed large parts of the forest stand and may remove evidence of past and subsequent events or disturb tree growth in such a way that younger events cannot be identified in the tree-ring record (e.g. Carrara, 1979; 1989; Kogelnig-Mayer et al., 2011). For example, we can reasonably attribute the clear temporal non-stationarity observed in the reconstructions (80% of the reconstructed events occurred during the 20th century and 36 out of 71 events even since 1960) to an increased potential to record past avalanche activity. This is related to the re-colonization of the 400 × 800-m forest strip destroyed by the January 1920 event and in which trees reached maturity only in the 1950s. Similarly we found a large number of trees showing GD as a result of the avalanche activity of 2012 and 2013, but failed to identify the event of March 4, 2014 that severely damaged the forest stand in T2 by uprooting, breaking or bending 165, 259, and 696 trees, respectively (Feistl et al., 2015); (iii) potential biases towards larger avalanches, as smaller snow avalanches or events limited to the non-forested parts of the avalanche system or strictly restricted to the incised Täschwang channel cannot be identified by means of tree-ring analysis; finally, (iv) our methodology is not normally able to provide a distinction between multiple events that occur at the same path during the same winter. As a consequence, and despite the stringency of the procedure employed in this paper, one has to keep in mind the number of reconstructed events has to be seen as a minimum frequency of natural avalanche activity.

On a spatial plan, past events were carefully delineated on the basis of growth disturbances observed in trees for a given year. Yet, limitations probably remain in the reconstruction of the boundaries of each event. In Chamonix, Corona et al. (2012) reported, by comparing archival records with tree-ring data, that runout distances tend to be underestimated with dendrogeomorphic techniques. Underestimations are attributed to (i) the modification of path geometry (steepness, curvature) by the geomorphic effect of the avalanches in the runout zone that may have induce rapid avalanche deceleration (McClung, 1990; McClung and Schaerer, 2006) and snow pressures that are insufficient to damage trees during some of the events; (ii) observation inaccuracies in historical archives, especially for old (Ancey, 2004) and extreme events involving very dry, non- cohesive snow and/or a powder cloud, for which the point of the farthest reach is sometimes very difficult to be located because of the absence of clearly visible deposits (Eckert et al.., 2010). As a consequence, we have to admit that the spatial patterns derived from our procedure contain some uncertainties that are not easily quantifiable and therefore have to be seen as the minimum yearly extent of avalanches that occurred in a given path.

5.2. From events to return period mapping

Dendrogeomorphology has a great potential to derive information on recurrence intervals of past avalanche events. Yet, only few studies (Fig. 1) really attempted to derive recurrence interval maps from tree-ring based reconstructions. In addition, by using an inaccurate definition of an avalanche return period, they usually failed to properly reproduce the expected patterns that typically increase as one moves down the avalanche path. In our study, Rim1 therefore is no exception to the rule. Classically based on the inverse distance weighting interpolation of individual tree recurrence intervals, the approach tends to homogenize recurrence intervals: a large part of the slope–with the exception of the release areas of T1 and at the outlet of the Täschwang channel (18–28 years)–are thus characterized by recurrence intervals that exceed 60 years with clear “bulls eye” effects. In addition, the map does not show a clear increase of recurrence intervals at the vicinity of the main channels. The limited value and lack of realistic representation of avalanche activity in these maps is also limited by the high spatial variability of recurrence intervals in individual trees which can in turn be explained by (i) the heterogeneity of GDs observed in trees for a given event (i.e. not all trees located in the flowpath of an avalanche will show a GD, see e.g. Fig. 9), but also (ii) by the number and

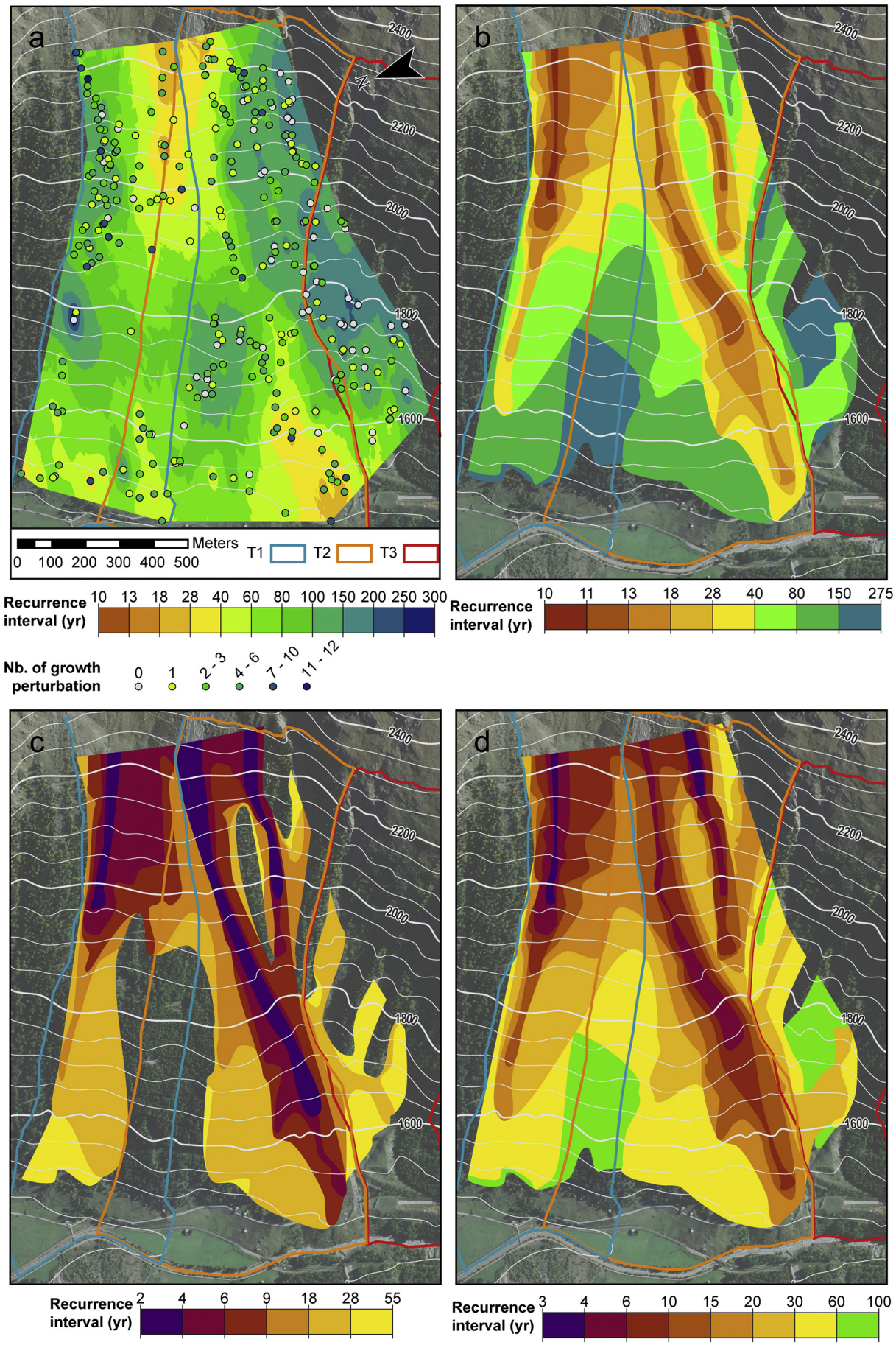

(caption on next page)

Fig. 10. (a) Interpolation of individual tree recurrence intervals (Rim1) often assimilated to avalanche return periods in the tree ring literature. Recurrence intervals computed according to the spatial delineation of past events based on growth disturbances in trees for the period 1740–2015 (Rim2, b) and 1960–2015 (Rim3, c). Map on panel (d) (Rim4) was transformed in order to adjust recurrence interval values from Rim2 and to estimate recurrence intervals in the missing portions of Rim3.

type of GDs recorded in each tree-ring series that directly depends on tree age (e.g. Šilhán and Stoffel, 2015) and tree species (Trappmann and Stoffel, 2013).

To overcome these biases, a new procedure was implemented in Rim2 and Rim3 that includes an expert delineation of past events based on disturbed trees. The resulting maps neither account for tree age nor do they involve interpolation processes. Instead, they represent a significant step towards a precise mapping of return period of avalanche events based on tree-ring analysis as they provide information on the time elapsing between two events for each location of the paths. Interestingly, they evidence similar patterns with highest recurrence intervals observed in the release areas of T1 and T2 and in the Täschwang channel. Owing to the non-stationarity of our reconstruction and to the increasing frequency of reconstructed snow avalanches for the last decades, the recurrence interval values of Rim2 (1740–2015) strongly exceed those computed for Rim3 (1961–2015). According to the limitations presented above for the early part of the reconstruction (see §5.2), we assume that Rim3 better estimates avalanche events recurrence intervals whereas Rim2 tends to strongly underestimate real avalanche activity as it only contains those snow avalanches that exceeded the boundaries of the 1920 extreme event, for example. Conversely, as no events could be retrieved in the lowermost part of the slope located between T1 and T2 since 1960, no recurrence interval could be computed at the interfluve between T1 and T2 on Rim3 which is more spatially limited. In order to (i) adjust recurrence interval values from Rim2 and to (ii) estimate the recurrence intervals in those parts not covered by Rim3, the distribution of the ratios Rim3/Rim2 was computed from those areas common to each map, and to then use the mean ratio (0.36) as a multiplier for Rim2. The composite recurrence interval map (Rim4, Fig. 10d) resulting from this transformation shows recurrence interval values > 60 yr at the interfluve between T1 and T2 and < 6 yr in the release areas of T2 and T3 and in the most active portions of the Täschwang channel. Interestingly, the latter values are in the same range as the recurrence intervals computed from historical documents for the period 1950–2000 (17 events, recurrence interval: 3 years) and 2000–2015 (3 events, recurrence interval 5 years).

Despite our efforts and encouraging results, we cannot consider at this stage that our recurrence interval maps can be readily used for hazard mapping purposes. Indeed, at a given location on the path, we compute the mean time separating two winters with at least one avalanche instead of the mean time between two snow avalanches which is more relevant for elements at risk. Even more critically, the above-mentioned limitations in terms of spatio-temporal accuracy of the approach makes the reliability of our maps still hampered by some uncertainties related to: (i) the detection of past events and the difficulty to estimate real avalanche activity from both archival records and tree-ring data; (ii) inaccuracies in the delineation of the boundaries of past events which can, e.g., lead to significant underestimations of real runout distances difficult to quantify and (iii) the fact that we cannot be sure that each point of the avalanche path is reached by one and unique release area. Nonetheless, however, results presented here should be used with care in combination with archival records, expert judgement and modeling output to maximize knowledge and confidence in proposed mitigation strategies.

6. Conclusion

In this study, we used dendrogeomorphic technics and historical archives to document past avalanche activity for three paths of the Täschwang avalanche system (Canton of Valais, Swiss Alps) with the specific aim to improve tree-ring based recurrence interval mapping. To this end, a 4-step procedure was used to retrieve evidence on 71 avalanche events for the period 1740–2014. The comparison between our reconstruction and historical archives reveals that 9 out of 16 (56%) avalanche years listed in local records could be reconstructed with tree-ring analysis. In addition, tree-ring analysis and archival records enabled attribution of the apparent increase in the frequency of snow avalanches observed after the 1950s to the extreme avalanche that occurred at Täschwang in 1920. By contrast to those classically found in the tree ring literature, the different recurrence interval maps derived from our reconstruction for different sub-periods (1720–2015 and 1960–2015) clearly show a realistic upslope-downslope gradient as well as lateral variations in recurrence intervals, with the highest values being observed in the main Täschwang channel. Despite further potential for refinement to improve and test the accuracy of our maps, e.g. by comparison with numerical simulations or classical hazard mapping procedures, this study demonstrates that dendrogeomorphic data should be seen as an extremely valuable data pool for avalanche hazard zoning on forested paths with limited or no historical data.

Acknowlegdment

The authors wish to address special thanks to Georges Tscherrig for his assistance in searching original newspaper articles. The authors acknowledge support from the Agence Nationale de la Recherche of the French government through the program “Investissements d'Avenir” (16-IDEX-0001 CAP 20-25). Finally, the authors acknowledge the two anonymous reviewers for their helpful and very positive comments on the manuscript and to Peter Gauer for the thorough editing.

References

Alestalo, J., 1971. Dendrochronological interpretation of geomorphic processes. Fennia 1–139.

Ancey, C., 2004. Powder snow avalanches: Approximation as non-Boussinesq clouds with a Richardson number–dependent entrainment function. J. Geophys. Res. Earth 109 (F1), F01005. http://dx.doi.org/10.1029/2003JF000052.

Ancey, C., Meunier, M., 2004. Estimating bulk rheological properties of flowing snow avalanches from field data. J. Geophys. Res. Earth 109, F01004. http://dx.doi.org/10.1029/2003JF000036.

Ancey, C., Gervasoni, C., Meunier, M., 2004. Computing extreme avalanches. Cold Reg. Sci. Technol. 39, 161–180. http://dx.doi.org/10.1016/j.coldregions.2004.04.004.

Arbellay, E., Stoffel, M., Decaulne, A., 2013. Dating of snow avalanches by means of wound-induced vessel anomalies in sub-arctic Betula pubescens. Boreas 42, 568–574. http://dx.doi.org/10.1111/j.1502-3885.2012.00302.x.

Badoux, A., Andres, N., Techel, F., Hegg, C., 2016. Natural hazard fatalities in Switzerland from 1946 to 2015. Nat. Hazards Earth Syst. 16, 2747–2768. http://dx.doi.org/10.5194/nhess-16-2747-2016.

Ballesteros-Cánovas, J.A., Trappmann, D., Madrigal-González, J., Eckert, N., Stoffel, M., 2018. Climate warming enhances snow avalanche risk in the western Himalayas. P. Natl. Acad. Sci. USA 115 (13), 3410–3415. http://dx.doi.org/10.1073/pnas.1716913115.

Baltensweiler, W., Benz, G., Bovey, P., Delucchi, V., 1977. Dynamics of larch bud moth populations. Annu. Rev. Entomol. 22, 79–100. http://dx.doi.org/10.1146/annurev.en.22.010177.000455.

Barbolini, M., Keylock, C.J., 2002. A new method for avalanche hazard mapping using a combination of statistical and deterministic models. Nat. Hazards Earth Syst. 2 (3–4), 239–245.

Barbolini, M., Gruber, U., Keylock, C.J., Naaim, M., Savi, F., 2000. Application of statistical and hydraulic-continuum dense-snow avalanche models to five real European sites. Cold Reg. Sci. Technol. 31 (2), 133–149. http://dx.doi.org/10.1016/S0165-232X(00)00008-2.

Bartelt, P., Salm, B., Gruber, U., 1999. Calculating dense-snow avalanche runout using a Voellmy-fluid model with active/passive longitudinal straining. J. Glaciol. 45 (150), 242–254. http://dx.doi.org/10.3189/S002214300000174X.

Battipaglia, G., Frank, D., Büntgen, U., Dobrovolný, P., Brázdil, R., Pfister, C., Esper, J., 2010. Five centuries of central European temperature extremes reconstructed from

tree-ring density and documentary evidence. Glob. Planet. Chang. 72, 182–191. http://dx.doi.org/10.1016/j.gloplacha.2010.02.004.
Boucher, D., Filion, L., Hétu, B., 2003. Reconstitution dendrochronologique et fréquence des grosses avalanches de neige dans un couloir subalpin du mont Hog's back, en Gaspésie Centrale (Québec). Géog. Phys. Quat. 57, 159–168. http://dx.doi.org/10.7202/011311ar.
Bozhinskiy, A.N., Nazarov, A.N., Chernouss, P.A., 2001. Avalanches: a probabilistic approach to modelling. Ann. Glaciol. 32, 255–258.
Bründl, M., Etter, H.J., Steiniger, M., Klingler, C., Rhyner, J., Ammann, W.J., 2004. IFKIS - a basis for managing avalanche risk in settlements and on roads in Switzerland. Nat. Hazards Earth Syst. 4, 257–262.
Bründl, M., Bartelt, P., Schweizer, J., Keiler, M., Glade, T., 2010. Review and future challenges in snow avalanche risk analysis. In: Alcántara-Ayala, I., Goudie, A. (Eds.), Geomorphological Hazards and Disaster Prevention. Cambridge University Press, Cambridge, pp. 49–61.
Bryant, C.L., Butler, D.R., Vitek, J.D., 1989. A statistical analysis of tree-ring dating in conjunction with snow avalanches: comparison of on-path versus off-path responses. Environ. Geol. Water Sci. 14, 53–59. http://dx.doi.org/10.1007/BF01740585.
Büntgen, U., Esper, J., Frank, D.C., Nicolussi, K., Schmidhalter, M., 2005. A 1052-year tree-ring proxy for alpine summer temperatures. Clim. Dyn. 25, 141–153. http://dx.doi.org/10.1007/s00382-005-0028-1.
Büntgen, U., Frank, D., Liebhold, A., Johnson, D., Carrer, M., Urbinati, C., Grabner, M., Nicolussi, K., Levanic, T., Espern, J., 2009. Three centuries of insect outbreaks across the European alps. New Phytol. 182, 929–941. http://dx.doi.org/10.1111/j.1469-8137.2009.02825.x.
Butler, D.R., 1979. Snow avalanche path terrain and vegetation, glacier National Park. Mont. Arctic Alpine Res. 11, 17–32. http://dx.doi.org/10.2307/1550456.
Butler, D.R., Malanson, G.P., 1985. A history of high-magnitude snow avalanches, southern glacier National Park, Montana, U.S.A. Mt. Res. Dev. 5, 175–182. http://dx.doi.org/10.2307/3673256.
Butler, D.R., Sawyer, C.F., 2008. Dendrogeomorphology and high-magnitude snow avalanches: a review and case study. Nat. Hazards Earth Syst. 8, 303–309. http://dx.doi.org/10.5194/nhess-8-303-2008.
Carrara, P.E., 1979. The determination of snow avalanche frequency through tree-ring analysis and historical records at Ophir, Colorado. Geol. Soc. Am. Bull. 90, 773–780. http://dx.doi.org/10.1130/0016-7606(1979)90<773:TDOSAF>2.0.CO;2.
Casteller, A., Stöckli, V., Villalba, R., Mayer, A.C., 2007. An evaluation of Dendroecological indicators of snow avalanches in the Swiss alps. Arct. Antarct. Alp. Res. 39, 218–228. http://dx.doi.org/10.1657/1523-0430(2007)39[218:AEODIO]2.0.CO;2.
Casteller, A., Christen, M., Villalba, R., Martínez, H., Stöckli, V., Leiva, J.C., Bartelt, P., 2008. Validating numerical simulations of snow avalanches using dendrochronology: the Cerro Ventana event in northern Patagonia, Argentina. Nat. Hazards Earth Syst. 8, 433–443.
Casteller, A., Villalba, R., Araneo, D., Stöckli, V., 2011. Reconstructing temporal patterns of snow avalanches at Lago del Desierto,southern Patagonian Andes. Cold Reg. Sci. Technol. 67, 68–78. http://dx.doi.org/10.1016/j.coldregions.2011.02.001.
Casteller, A., Häfelfinger, T., Cortés Donoso, E., Podvin, K., Kulakowski, D., Bebi, P., 2018. Assessing the interaction between mountain forests and snow avalanches at Nevados de Chillán, Chile and its implications for ecosystem-based disaster risk reduction. Nat. Hazards Earth Syst. Sci. 18, 1173–1186. http://dx.doi.org/10.5194/nhess-18-1173-2018.
Chiroiu, P., Stoffel, M., Onaca, A., Urdea, P., 2015. Testing dendrogeomorphic approaches and thresholds to reconstruct snow avalanche activity in the Făgăraş Mountains (Romanian Carpathians). Quat. Geochronol. 27, 1–10. http://dx.doi.org/10.1016/j.quageo.2014.11.001.
Corona, C., Rovéra, G., Lopez-Saez, J., Stoffel, M., Perfettini, P., 2010. Spatio-temporal reconstruction of snow avalanche activity using tree rings: Pierres Jean Jeanne avalanche talus, massif de l'Oisans, France. Catena 83, 107–118. http://dx.doi.org/10.1016/j.catena.2010.08.004.
Corona, C., Lopez-Saez, J., Stoffel, M., Bonnefoy, M., Richard, D., Astrade, L., Berger, F., 2012. How much of the real avalanche activity can be captured with tree rings? an evaluation of classic dendrogeomorphic approaches and comparison with historical archives. Cold Reg. Sci. Technol. 74–75, 31–42. http://dx.doi.org/10.1016/j.coldregions.2012.01.003.
Corona, C., Lopez-Saez, J., Stoffel, M., Rovéra, G., Edouard, J.-L., Berger, F., 2013. Seven centuries of avalanche activity at Echalp (Queyras massif, southern French alps) as inferred from tree rings. The Holocene 23 (2), 292–304. http://dx.doi.org/10.1177/0959683612460784.
Dale, M.R.T., Fortin, M.-J., 2014. Spatial Analysis: A Guide for Ecologists, 2nd edn. Cambridge University Press, Cambridge.
Decaulne, A., Eggertsson, Ó., Sæmundsson, Þ., 2012. A first dendrogeomorphologic approach of snow avalanche magnitude–frequency in northern Iceland. Geomorphology 167–168, 35–44. http://dx.doi.org/10.1016/j.geomorph.2011.11.017.
Decaulne, A., Eggertsson, Ó., Laute, K., Beylich, A.A., 2014. A 100-year extreme snow-avalanche record based on tree-ring research in upper Bødalen, inner Nordfjord, western Norway. Geomorphology 218, 3–15. http://dx.doi.org/10.1016/j.geomorph.2013.12.036.
Van Der Burght, L., Stoffel, M., Bigler, C.J., 2012. Analysis and modelling of tree succession on a recent rockslide deposit. Plant Ecol. 213, 35–46.
Dubé, S., Filion, L., Hétu, B., 2004. Tree-ring reconstruction of high-magnitude snow avalanches in the northern Gaspé peninsula, Québec, Canada. Arct. Antarct. Alp. Res. 36, 555–564. http://dx.doi.org/10.1657/1523-0430(2004)036[0555:TROHSA]2.0.CO;2.
Eckert, N., Parent, E., Richard, D., 2007. Revisiting statistical–topographical methods for avalanche predetermination: Bayesian modelling for runout distance predictive distribution. Cold Reg. Sci. Technol. 49 (1), 88–107. http://dx.doi.org/10.1016/j.coldregions.2007.01.005.
Eckert, N., Parent, E., Naaim, M., Richard, D., 2008. Bayesian stochastic modelling for avalanche predetermination: from a general system framework to return period computations. Stoch. Env. Res. Risk A. 22 (2), 185–206. http://dx.doi.org/10.1007/s00477-007-0107-4.
Eckert, N., Naaim, M., Parent, E., 2010. Long-term avalanche hazard assessment with a Bayesian depth-averaged propagation model. J. Glaciol. 56 (198), 563–586. http://dx.doi.org/10.3189/002214310793146331.
Efthymiadis, D., Jones, P.D., Briffa, K.R., Auer, I., Böhm, R., Schöner, W., Frei, C., Schmidli, J., 2006. Construction of a 10-min-gridded precipitation data set for the greater alpine region for 1800–2003. J. Geophys. Res. 111. http://dx.doi.org/10.1029/2005JD006120.
Esper, J., Buntgen, U., Frank, D.C., Nievergelt, D., Liebhold, A., 2007. 1200 years of regular outbreaks in alpine insects. Proc. R. Soc. B Biol. Sci. 274, 671–679. http://dx.doi.org/10.1098/rspb.2006.0191.
ESRI, 2013. ArcGIS 10.2. ESRI, Redlands, CA.
Favillier, A., Guillet, S., Morel, P., Corona, C., Lopez-Saez, J., Eckert, N., Ballesteros-Cánovas, J.A., Peiry, J.-L., Stoffel, M., 2017. Disentangling the impacts of exogenous disturbances on forest stands to assess multi-centennial tree-ring reconstructions of avalanche activity in the upper Goms Valley (Canton of Valais, Switzerland). Quat. Geochronol. 42, 89–104. http://dx.doi.org/10.1016/j.quageo.2017.09.001.
Feistl, T., Bebi, P., Christen, M., Margreth, S., Diefenbach, L., Bartelt, P., 2015. Forest damage and snow avalanche flow regime. Nat. Hazards Earth Syst. 15, 1275–1288. http://dx.doi.org/10.5194/nhess-15-1275-2015.
Frazer, G.H., 1985. Dendrogeomorphic Evaluation of Snow Avalanche History at two Sites in Banff National Park. Department of Geography, University of Western Ontario, London, ON, Canada.
Gadek, B., Kaczka, R.J., Rączkowska, Z., Rojan, E., Casteller, A., Bebi, P., 2017. Snow avalanche activity in Żleb Żandarmerii in a time of climate change (Tatra Mts., Poland). Catena 158, 201–212. http://dx.doi.org/10.1016/j.catena.2017.07.005.
Garavaglia, V., Pelfini, M., 2011. The role of border areas for dendrochronological investigations on catastrophic snow avalanches: a case study from the Italian alps. Catena 87, 209–215. http://dx.doi.org/10.1016/j.catena.2011.06.006.
George, J.-P., Grabner, M., Karanitsch-Ackerl, S., Mayer, K., Weißenbacher, L., Schueler, S., 2017. Genetic variation, phenotypic stability, and repeatability of drought response in European larch throughout 50 years in a common garden experiment. Tree Physiol. 37 (1), 33–46. http://dx.doi.org/10.1093/treephys/tpw085.
Germain, D., 2016. A statistical framework for tree-ring reconstruction of high-magnitude mass movements: case study of snow avalanches in eastern Canada. Geogr. Ann. Ser. Phys. Geogr. 98 (4), 303–311. http://dx.doi.org/10.1111/geoa.12138.
Germain, D., Filion, L., Hétu, B., 2005. Snow avalanche activity after fire and logging disturbances, northern Gaspé peninsula, Quebec, Canada. Can. J. Earth Sci. 42, 2103–2116.
Germain, D., Filion, L., Hétu, B., 2009. Snow avalanche regime and climatic conditions in the chic-choc range, eastern Canada. Clim. Chang. 92, 141–167. http://dx.doi.org/10.1007/s10584-008-9439-4.
Hebertson, E.G., Jenkins, M.J., 2003. Historic climate factors associated with major avalanche years on the Wasatch plateau, Utah. Cold Reg. Sci. Technol. 37, 315–332. http://dx.doi.org/10.1016/S0165-232X(03)00073-9.
Ives, J.D., Mears, A.I., Carrara, P.E., Bovis, M.J., 1976. Natural hazards in mountain Colorado. Ann. Assoc. Am. Geogr. 66, 129–144. http://dx.doi.org/10.1111/j.1467-8306.1976.tb01076.x.
Jenkins, M.J., Hebertson, E.G., 2004. A practitioner's guide for using dendroecological techniques to determine the extent and frequency of avalanches. In: Proceedings of the International Snow Science Workshop. Jackson, Wyoming, Jackson, pp. 423–431.
Kajimoto, T., Daimaru, H., Okamoto, T., Otani, T., Onodera, H., 2004. Effects of snow avalanche disturbance on regeneration of subalpine Abies mariesii forest, northern Japan. Arct. Antarct. Alp. Res. 36, 436–445.
Kennedy, M.D., 2013. Introducing Geographic Information Systems with ARCGIS: A Workbook Approach to Learning GIS, 3rd edn. John Wiley & Sons, Hoboken.
Keylock, C.J., 2005. An alternative form for the statistical distribution of extreme avalanche runout distances. Cold Reg. Sci. Technol. 42 (3), 185–193. http://dx.doi.org/10.1016/j.coldregions.2005.01.004.
Kogelnig-Mayer, B., Stoffel, M., Schneuwly-Bollschweiler, M., Hübl, J., Rudolf-Miklau, F., 2011. Possibilities and limitations of Dendrogeomorphic time-series reconstructions on sites influenced by debris flows and frequent snow avalanche activity. Arct. Antarct. Alp. Res. 43, 649–658. http://dx.doi.org/10.1657/1938-4246-43.4.649.
Kogelnig-Mayer, B., Stoffel, M., Schneuwly-Bollschweiler, M., 2013. Four-dimensional growth response of mature Larix decidua to stem burial under natural conditions. Trees 27, 1217–1223. http://dx.doi.org/10.1007/s00468-013-0870-4.
Köse, N., Aydın, A., Akkemik, Ü., Yurtseven, H., Güner, T., 2010. Using tree-ring signals and numerical model to identify the snow avalanche tracks in Kastamonu, Turkey. Nat. Hazards 54, 435–449. http://dx.doi.org/10.1007/s11069-009-9477-x.
Krause, D., Křížek, M., 2017. Dating of recent avalanche events in the eastern high Sudetes, Czech Republic. Quat. Int. 470, 166–175. http://dx.doi.org/10.1016/j.quaint.2017.09.001.
Kress, A., Saurer, M., Büntgen, U., Treydte, K.S., Bugmann, H., Siegwolf, R.T.W., 2009. Summer temperature dependency of larch budmoth outbreaks revealed by alpine tree-ring isotope chronologies. Oecologia 160, 353–365. http://dx.doi.org/10.1007/s00442-009-1290-4.
Larocque, S.J., Hétu, B., Filion, L., 2001. Geomorphic and dendroecological impacts of slushflows in Central Gaspé peninsula (Québec, Canada). Geogr. Ann. Ser. Phys. Geogr. 83, 191–201. http://dx.doi.org/10.1111/j.0435-3676.2001.00154.x.
Laternser, M., Pfister, C., 1997. Avalanches in Switzerland 1500-1990. In: Frenzel, B., Matthews, J., Gläser, A., Weiss, M. (Eds.), Rapide Mass Movement since the

Holocene. Palaeoclimate Research, pp. 241–266.
Laxton, S.C., Smith, D.J., 2009. Dendrochronological reconstruction of snow avalanche activity in the Lahul Himalaya, Northern India. Nat. Hazards 49, 459–467. http://dx.doi.org/10.1007/s11069-008-9288-5.
Lempa, M., Kaczka, R.J., Rączkowska, Z., Janecka, K., 2016. Combining tree-ring dating and geomorphological analyses in the reconstruction of spatial patterns of the runout zone of snow avalanches, Rybi Potok Valley, Tatra Mountains (Poland). Geogr. Pol. 89 (1), 31–45. http://dx.doi.org/10.7163/GPol.0044.
Lévesque, M., Saurer, M., Siegwolf, R., Eilmann, B., Brang, P., Bugmann, H., Rigling, A., 2013. Drought response of five conifer species under contrasting water availability suggests high vulnerability of Norway spruce and European larch. Glob. Chang. Biol. 19 (10), 3184–3199. http://dx.doi.org/10.1111/gcb.12268.
Lied, K., Bakkehøi, K., 1980. Empirical calculations of snow–avalanche run–out distance based on topographic parameters. J. Glaciol. 26 (94), 165–177. http://dx.doi.org/10.3189/S0022143000010704.
Maggioni, M., Gruber, U., Purves, R.S., Freppaz, M., 2006. Potential release areas and return period of avalanches: is there a relation? In: Sternbenz, C., Greene, N. (Eds.), Proceedings of the 2006 International Snow Science Workshop. Telluride, Colorado, Telluride, pp. 566–571.
Martin, J.-P., Germain, D., 2016a. Can we discriminate snow avalanches from other disturbances using the spatial patterns of tree-ring response? Case studies from the presidential range, White Mountains, New Hampshire, United States. Dendrochronologia 37, 17–32. http://dx.doi.org/10.1016/j.dendro.2015.12.004.
Martin, J.-P., Germain, D., 2016b. Dendrogeomorphic reconstruction of snow avalanche regime and triggering weather conditions: a classification tree model approach. Prog. Phys. Geogr. 40, 527–548. http://dx.doi.org/10.1177/0309133315625863.
McClung, D.M., 1990. A model for scaling avalanche speeds. J. Glaciol. 36 (123), 188–198. http://dx.doi.org/10.3189/S0022143000009436.
McClung, D.M., Lied, K., 1987. Statistical and geometrical definition of snow avalanche runout. Cold Reg. Sci. Technol. 13 (2), 107–119. http://dx.doi.org/10.1016/0165-232X(87)90049-8.
McClung, D.M., Schaerer, P.A., 2006. The Avalanche Handbook, 2nd edn. The Mountaineers Books, Seattle.
Meunier, M., Ancey, C., 2004. Towards a conceptual approach to predetermining long-return-period avalanche run-out distances. J. Glaciol. 50 (169), 268–278. http://dx.doi.org/10.3189/172756504781830178.
Mundo, I.A., Barrera, M.D., Roig, F.A., 2007. Testing the utility of Nothofagus pumilio for dating a snow avalanche in Tierra del Fuego, Argentina. Dendrochronologia 25, 19–28. http://dx.doi.org/10.1016/j.dendro.2007.01.001.
Muntán, E., Andreu, L., Oller, P., Gutiérrez, E., Martínez, P., 2004. Dendrochronological study of the canal del roc Roig avalanche path: first results of the Aludex project in the Pyrenees. Ann. Glaciol. 38, 173–179. http://dx.doi.org/10.3189/172756404781815077.
Muntán, E., Garcia, C., Oller, P., Martí, G., Garcia, A., Gutiérrez, E., 2009. Reconstructing snow avalanches in the southeastern Pyrenees. Nat. Hazards Earth Syst. 9, 1599–1612.
Pederson, G.T., Reardon, B.A., Caruso, C.J., Fagre, D.B., 2006. High resolution tree-ring based spatial reconstructions of snow avalanche activity in glacier national park, Montana, USA. In: Sterbenz, C., Greene, N. (Eds.), Proceedings of the International Snow Science Workshop. Telluride, Colorado. Telluride, pp. 436–443.
Pop, O.T., Gavrilă, I.-G., Roşian, G., Meseşan, F., Decaulne, A., Holobâcă, I.H., Anghel, T., 2016. A century-long snow avalanche chronology reconstructed from tree-rings in Parâng Mountains (southern Carpathians, Romania). Quat. Int. 415, 230–240. http://dx.doi.org/10.1016/j.quaint.2015.11.058.
Pop, O.T., Munteanu, A., Meseşan, F., Gavrilă, I.-G., Cosmin, T., Holobâcă, I.H., 2017. Tree-ring-based reconstruction of high-magnitude snow avalanches in Piatra Craiului Mountains (Southern Carpathians, Romania). Geogr. Ann. Ser. A 1–17. http://dx.doi.org/10.1080/04353676.2017.1405715.
Potter, N., 1969. Tree-ring dating of snow avalanche tracks and the geomorphic activity of avalanches, northern Absaroka Mountains, Wyoming. Geol. Soc. Am. Spec. Pap. 123, 141–166. http://dx.doi.org/10.1130/SPE123-p141.
Rayback, S.A., 1998. A Dendrogeomorphological analysis of snow avalanches in the Colorado front range, USA. Phys. Geogr. 19, 502–515. http://dx.doi.org/10.1080/02723646.1998.10642664.
Reardon, B.A., Pederson, G.T., Caruso, C.J., Fagre, D.B., 2008. Spatial reconstructions and comparisons of historic snow avalanche frequency and extent using tree rings in glacier National Park, Montana, U.S.A. Arct. Antarct. Alp. Res. 40, 148–160. http://dx.doi.org/10.1657/1523-0430(06-069)[REARDON]2.0.CO;2.
Salm, B., Burkard, A., Gubler, H., 1990. Berechnung von fliesslawinen: eine Anleitung für praktiker mit beispielen. In: Mitteilung 47. Eidgenossichen Institut für Schnee- und, Lawinenforschung SLF, Davos.
Schaerer, P.A., 1972. Terrain and vegetation of snow avalanche sites at Rogers Pass, British Columbia in Mountain Geomorphology. In: Slaymaker, O., McPherson, H.J. (Eds.), Mountain Geomorphology: Geomorphological Processes in the Canadian Cordillera. Vancouver B.C., Vancouver, pp. 215–222.
Schläppy, R., Jomelli, V., Grancher, D., Stoffel, M., Corona, C., Brunstein, D., Eckert, N., Deschatres, M., 2013. A new tree-ring-based, semi-quantitative approach for the determination of snow avalanche events: use of classification trees for validation. Arct. Antarct. Alp. Res. 45, 383–395. http://dx.doi.org/10.1657/1938-4246-45.3.383.
Schläppy, R., Eckert, N., Jomelli, V., Stoffel, M., Grancher, D., Brunstein, D., Naaim, M., Deschatres, M., 2014. Validation of extreme snow avalanches and related return periods derived from a statistical-dynamical model using tree-ring techniques. Cold Reg. Sci. Technol. 99, 12–26. http://dx.doi.org/10.1016/j.coldregions.2013.12.001.
Schläppy, R., Jomelli, V., Eckert, N., Stoffel, M., Grancher, D., Brunstein, D., Corona, C., Deschatres, M., 2016. Can we infer avalanche–climate relations using tree-ring data? Case studies in the French alps. Reg. Environ. Chang. 16 (3), 629–642. http://dx.doi.org/10.1007/s10113-015-0823-0.
Schneuwly, D.M., Stoffel, M., Bollschweiler, M., 2008. Formation and spread of callus tissue and tangential rows of resin ducts in Larix decidua and Picea abies following rockfall impacts. Tree Physiol. 29, 281–289. http://dx.doi.org/10.1093/treephys/tpn026.
Schneuwly, D.M., Stoffel, M., Dorren, L.K.A., Berger, F., 2009. Three-dimensional analysis of the anatomical growth response of European conifers to mechanical disturbance. Tree Physiol. 29, 1247–1257. http://dx.doi.org/10.1093/treephys/tpp056.
Shroder, J., 1978. Dendrogeomorphological analysis of mass movement on Table Cliffs Plateau, Utah. Quat. Res. 9, 168–185. http://dx.doi.org/10.1016/0033-5894(78)90065-0.
Šilhán, K., Stoffel, M., 2015. Impacts of age-dependent tree sensitivity and dating approaches on dendrogeomorphic time series of landslides. Geomorphology 236, 34–43. http://dx.doi.org/10.1016/j.geomorph.2015.02.003.
Šilhán, K., Tichavský, R., 2017. Snow avalanche and debris flow activity in the high Tatras Mountains: new data from using dendrogeomorphic survey. Cold Reg. Sci. Technol. 134, 45–53. http://dx.doi.org/10.1016/j.coldregions.2016.12.002.
Smith, L., 1973. Indication of snow avalanche periodicity through interpretation of vegetation patterns in the North Cascades, Washington. In: Brown, C.B., Evans, R.J., Fox, T., LaChapelle, E.R., McClung, D.M., Smith, L. (Eds.), Methods of Avalanche Control on Washington Mountain Highways–Third Annual Report. Washington State Highway Commission Department of Highways, pp. 55–101.
Stoffel, M., Bollschweiler, M., 2008. Tree-ring analysis in natural hazards research–an overview. Nat. Hazards Earth Syst. 8, 187–202. http://dx.doi.org/10.5194/nhess-8-187-2008.
Stoffel, M., Corona, C., 2014. Dendroecological dating of geomorphic disturbance in trees. Tree-Ring Res. 70, 3–20. http://dx.doi.org/10.3959/1536-1098-70.1.3.
Stoffel, M., Bollschweiler, M., Hassler, G.-R., 2006. Differentiating past events on a cone influenced by debris-flow and snow avalanche activity – a dendrogeomorphological approach. Earth Surf. Process. Landf. 31, 1424–1437. http://dx.doi.org/10.1002/esp.1363.
Stoffel, M., Bollschweiler, M., Butler, D.R., Luckman, B., 2010. Tree Rings and Natural Hazards. Springer, Dordrecht, New York.
Stoffel, M., Butler, D.R., Corona, C., 2013. Mass movements and tree rings: a guide to dendrogeomorphic field sampling and dating. Geomorphology 200, 106–120. http://dx.doi.org/10.1016/j.geomorph.2012.12.017.
Straub, D., Grêt-Regamey, A., 2006. A Bayesian probabilistic framework for avalanche modelling based on observations. Cold Reg. Sci. Technol. 46 (3), 192–203. http://dx.doi.org/10.1016/j.coldregions.2006.08.024.
Szymczak, S., Bollschweiler, M., Stoffel, M., Dikau, R., 2010. Debris-flow activity and snow avalanches in a steep watershed of the Valais alps (Switzerland): Dendrogeomorphic event reconstruction and identification of triggers. Geomorphology 116 (1–2), 107–114. http://dx.doi.org/10.1016/j.geomorph.2009.10.012.
Techel, F., Stucki, T., Margreth, S., Marty, C., Winkler, K., 2015. Schnee und Lawinen in den Schweizer Alpen: Hydrologisches Jahr 2013/14 (No. 31). WSL-Insitut für Schnee- und Lawinenforschung, Birmensdorf.
Trappmann, D., Stoffel, M., 2013. Counting scars on tree stems to assess rockfall hazards: a low effort approach, but how reliable? Geomorphology 180–181, 180–186. http://dx.doi.org/10.1016/j.geomorph.2012.10.009.
Tumajer, J., Treml, V., 2015. Reconstruction ability of dendrochronology in dating avalanche events in the Giant Mountains, Czech Republic. Dendrochronologia 34, 1–9. https://doi.org/10.1016/j.dendro.2015.02.002.
Voellmy, A., 1955. Uber die Zerstrungskraft von Lawinen. Schweiz. Bauzig. (73(12/15/17/19), 159–162, 212–217, 246–249, 280–285).
Voiculescu, M., Onaca, A., 2013. Snow avalanche assessment in the Sinaia ski area (Bucegi Mountains, southern Carpathians) using the dendrogeomorphology method. Area 45, 109–122. http://dx.doi.org/10.1111/area.12003.
Voiculescu, M., Onaca, A., 2014. Spatio-temporal reconstruction of snow avalanche activity using dendrogeomorphological approach in Bucegi Mountains Romanian Carpathians. Cold Reg. Sci. Technol. 104–105, 63–75. http://dx.doi.org/10.1016/j.coldregions.2014.04.005.
Voiculescu, M., Onaca, A., Chiroiu, P., 2016. Dendrogeomorphic reconstruction of past snow avalanche events in Bâlea glacial valley–Făgăraş massif (southern Carpathians), Romanian Carpathians. Quat. Int. 415, 286–302. http://dx.doi.org/10.1016/j.quaint.2015.11.115.